NUREG/CR-3281
BNL-NUREG-51670

Investigation of Shell Cracking on the Steam Generators at Indian Point Unit No. 3

Prepared by C. J. Czajkowski

Brookhaven National Laboratory

Prepared for
U.S. Nuclear Regulatory Commission

GPO Printed copy price: $4.00

NUREG/CR-3281
BNL-NUREG-51670

Investigation of Shell Cracking on the Steam Generators at Indian Point Unit No. 3

Manuscript Completed: April 1983
Date Published: June 1983

Prepared by
C. J. Czajkowski

Brookhaven National Laboratory
Department of Nuclear Energy
Upton, NY 11973

Prepared for
Division of Engineering
Office of Nuclear Reactor Regulation
U.S. Nuclear Regulatory Commission
Washington, D.C. 20555
NRC FIN A3400

ABSTRACT

A metallurgical investigation was performed on specimens from the shell of steam generators #31 and 32 of the Indian Point 3 Power Plant. The examination consisted of optical microscopy, SEM/EDS, hardness measurements, and two different heat treatments. The shell material exhibited high values in hardness prior to the heat treatments, which was indicative that relatively high residual stresses may have been present in the areas of the welds. All observed cracks were transgranular in appearance and were associated with pits on the vessel's inside surfaces. Beach marks were observed on a fracture face from steam generator #32, as well as possible fatigue striations.

The report concludes that the cracking was caused by a low cycle corrosion fatigue phenomenon with cracks initiating at areas of localized corrosion and propagating by fatigue. The cause of the pitting/cracking is considered to be related to the unit's relatively high operating O_2 levels and copper species in solution. The report also concludes that stress corrosion cracking cannot be entirely discounted as a possible failure mechanism.

TABLE OF CONTENTS

LIST OF TABLES

LIST OF GRAPHS

LIST OF FIGURES

LIST OF FIGURES
(Cont'd)

LIST OF FIGURES
(Cont'd)

I. INTRODUCTION

On March 27, 1982, during a refueling outage (with the reactor in a cold shutdown condition), a small leak was detected on the shell side of steam generator #32 at the Indian Point-3 Nuclear Power Plant. Further examination of steam generator #32 disclosed that the detected leak originated in the circumferential weld joining the transition cone to the upper shell (closure weld) of the steam generator (Figure 1).

Indian Point-3 is a 925 MWe pressurized water reactor (PWR) with four Westinghouse Model 44 steam generators (vertical U-tube design). The unit has had approximately three years of effective full power operation since its commercial starting date in 1976.

The steam generator shell is constructed of SA302 Grade B material (Table 1) of 4" approximate thickness. The closure weld had a nominal 45° included angle weld preparation and was welded from the outside surface of the vessel by the submerged arc process with backing. The spacer strip was then back-gouged and the weld completed by welding from the inside surface with the shielded metal arc (SMAW) process using E8018-C3 electrode (Table 2). The weld was then continuously stress relieved at 1000°F minimum for three hours/inch of thickness (12 hours total soak time).

Closer examination of the area of the leak disclosed a hole on the outer surface of steam generator #32 approximately 16 mm long by 5 mm wide (Figure 2). The owner of Indian Point-3, Power Authority of the State of New York (PASNY), then instituted a nondestructive testing program consisting of visual inspection, ultrasonic examination, and magnetic particle examination of the affected welds. These examinations disclosed that the closure weld on each of the steam generators had in excess of 100 cracks associated with them, although the only through-crack was the "leaker" in steam generator #32. A significant amount of pitting (Figure 3) was also associated with the closure welds of the steam generator inside surfaces.

In order to characterize the cracking, PASNY had a 4" x 1" elliptically shaped boat sample (containing circumferentially oriented cracks) removed from the inside surface of steam generator #32 in the area of the closure weld. This sample was first sent to Lucius Pitkin, Inc. and then to General Electric Co. for metallurgical evaluation and failure analyses. These analyses yielded somewhat differing conclusions as to the cause of the cracking. Another larger sample (6" plug) was removed from steam generator #32 encompassing the through wall leaker (Figures 2 and 3), and sent to Lucius Pitkin for further analysis. Owing to the possible "generic" nature of the problem, the Westinghouse Corporation recommended that certain plants initiate inspections of their PWR steam generators during their scheduled shutdowns. Additionally, the Materials Engineering Branch (MTEB) of the United States Nuclear Regulatory Commission (USNRC) commissioned Brookhaven National Laboratory (BNL) to perform an independent failure analysis on the 6" plug (after completion of the evaluation by Lucius Pitkin), and on three additional boat samples containing cracks cut from steam generator #31.

The BNL evaluation was to encompass the following tasks in order to determine the possible cause(s) of the cracking:

1) Visual examination/photography
2) Hardness measurements/heat treatment
3) Optical microscopy
4) Scanning electron microscopy (SEM)/energy dispersive spectroscopy (EDS)

These examinations were performed on both the plug specimens and the three boat samples.

II. VISUAL EXAMINATION

Figure 4 is a section of the 6" plug removed from steam generator #32. It is cut vertically, relative to the steam generator weld. The section was etched for one minute using a 10% ammonium persulfate + water etch. The multiple weld passes of the crown weld are clearly seen, as well as a large area of repair weld at the inside surface. A crack approximately 20 mm in length is visible on the upper shell side of the weld 6 mm away from the repair weld heat affected zone (HAZ). Circled section A in Figure 4 is an area of lack of fusion (higher magnification micrographs are in optical microscopy section) which did not appear to propagate. Area B is an area of porosity which is related to the original repair welding of the steam generator vessel.

The actual path of the through wall "leaker" seemingly followed the weld heat affected zone and is clearly defined in Figure 5. The broadening of the crack near the outside surface of the steam generator is most probably the result of a steam channel erosion effect after the crack had breached the outer surface.

Figure 6 is a macrophotograph of another specimen received from Lucius Pitkin depicting the relative location of another crack to the repair weld area.

All three of the boat samples received from PASNY (Figures 7, 8 and 9) showed evidence of pitting on the inside surface of the steam generator, especially in the case of MT indications 44 and 46, whose cracks appeared as an array of pits following the crack outline.

III. HARDNESS MEASUREMENTS/HEAT TREATMENT

The section of plug weld (Figure 4) was polished and etched and then microhardness measurements were performed on the specimen as received. Table 3 is a tabulation of these measurements. Additionally, Rockwell measurements were performed for comparison of the weldments' bulk properties. The plug section was then subjected to two differing heat treatments:

a) 1000°F for 3 hours/inch of thickness with a cooling rate not exceeding 100°F/hour until 600°F, then furnace-cooled.

b) 1125°F for 1 hour/inch of thickness with a cooling rate not exceeding 100°F/hour until 600°F, then furnace-cooled.

Hardness measurements (both Knoop and Rockwell) were taken after each heat treatment and are also listed in Table 3. All values recorded for the base metal, weld metal and heat affected areas were then plotted on Graphs 1-3. The solid line in each graph represents the maximum hardness values recorded, while the dashed line is the simple arithmetical average of the recorded values. It is evident from the three tables that each of the heat treatments reduced not only the maximum hardness values, but also the average hardness values recorded.

These results indicate that this particular section of the plug weld had received a heat treatment of less than 1000°F in the location of the hardness measurements. This reduction of maximum and average hardness values after heat treatment were also substantiated by the Rockwell measurements. The only exception to this was that the maximum value of the base metal hardness measurements appeared to increase slightly after the 1000°F heat treatment. This increase was well within the sensitivity range of the equipment. The highest value obtained during these tests was KHN 367, or the equivalent of R_C 36.6, which is not inordinately high for this material in the as-welded condition.

Table 4 is a tabulation of microhardness readings for the three coat samples removed from steam generator #31. A maximum value of KHN 396 was recorded, translating to R_C 39.4. This peak value is an indication that relatively high residual welding stresses may be present in this weldment.

IV. OPTICAL MICROSCOPY

Various pits on the inside surface of the plug sample were examined by optical microscopy after etching with a 10% Nital solution. The specimens were prepared by making a cut perpendicular to the inside surface of the plug and then grinding and polishing back until the pits were reached. Some pits examined (Figure 10) had no cracks associated with them. The structure of the material in the area adjacent to the pits was that of a tempered martensite, which would be normal for this type of steel.

Some shallow pits had cracks associated with them (Figures 11 and 12). The cracks were tight and transgranular in nature, emanating at the bottom of the shallow pits. These cracks were continuous with virtually no branching evident. Other pits had shallow, opened-mouthed cracks associated with them (Figures 13 and 14). These cracks had the appearance of having a more active corrosion process associated with them than the predominantly transgranular ones. The microstructure surrounding these cracks was also a tempered martensite.

The area of lack of fusion in Figure 4 (area A) was also investigated. Figure 15 is a photomicrograph showing the area of lack of fusion (boxed area) in relation to the weld and heat affected zone of the repair weld. Figure 16 is a higher magnification photomicrograph showing that no subcracks are associated with the area of lack of fusion.

The microstructure of the various base metals (Figure 17), weld metals (Figure 18) and heat affected zones (Figure 19) from the 6" plug were examined. The base metal had a tempered martensitic structure consistent with A302 Grade B material. The weld metal had a dendritic structure which would be normal for both manually deposited shielded metal arc weld of E8018-C3 material and submerged arc welding. The heat affected zone of the plug weld had a more acicular structure normally associated with untempered martensite.

A comparison (Figure 20) photomicrograph/fractograph was made of the crack shown in the specimen in Figure 6. It is quite evident that the crack is transgranular with virtually no branching associated with it. Although there is no definitive heat affected zone visible in the immediate vicinity of this crack, there was a grain size difference between areas closer to the inner surface and those about mid-depth of the crack. This grain size difference is similar to that which would normally be associated with weld heat affected zones or those encountered with mechanically worked thick sections in materials. The fractograph clearly shows a non-continuous crack growth initiating from a point on the fracture surface not included on the fractograph due to the limited thickness of this particular specimen. The radiating lines in the upper section of the fractograph would normally point to the initiation site of the fracture.

Optical cross sections were cut, mounted and etched from the three boat samples cut from steam generator #31. Figure 21 shows the crack identified as MT indication #37. The crack is extremely straight, transgranular, and exhibits virtually no crack branching. The crack appears to initiate at a pit on the inside surface of the specimen. The higher magnification photomicrographs of the weld metal (Figure 21a) shows a normal dendritic structure for E8018-C3 material. The base metal had a tempered martensitic structure (Figure 21b) which is also normal for the material condition. Figure 21c is a photomicrograph of the heat affected zone which has a more acicular structure not normally associated with the "tempered martensitic" condition, but more normally associated with untempered martensite.

The cracks associated with MT indications 44 (Figure 22) and 46 (Figure 23) were both associatd with surface pits and were transgranular with very little branching evident. Both cracks exhibited arrests along their length where it appears that the corrosion process was dominant for some period of time. The higher magnification photomicrographs (Figures 22a,b,c, and 23a,b,c) of the base metal, weld metal and heat affected zone structure of these two cracks correspond to the same observations noted previously on MT indication #37.

V. SEM/EDS

Various fracture faces from both the plug and the three boat samples were examined, in the hope of characterizing the failure mode. Additionally, the fracture faces and various pits were examined by Energy Dispersive Spectroscopy (EDS) in an attempt to determine if corrosive constituents were present.

The first specimens examined were those from the 6" plug. Initial examination of the fracture faces disclosed that the surfaces were covered by a tight and adherent oxide film. In order to more fully characterize the fractographic features of the cracks, an electrolytic cleaning procedure was instituted on the plug weld specimens. This cleaning procedure is described below. A working solution of Endox-214 was prepared by adding 8 ounces of Endox-214 powder to 1000 ml of cold water and stirring until it was completely dissolved. A small amount of Photoflow was added to the solution to aid the wetting of the specimen and eliminate some of the featuring during the electrochemical cleaning step. A glass beaker with 500 ml of the Endox-214 solution was placed in an ultrasonic cleaner. The specimen was made the cathode, and a platinum wire loop used as an anode. A current density of ~ 250 mA/cm^2 was applied for 15 seconds. The specimen was removed from the electrolyte and ultrasonically washed in a detergent solution consisting of Alconox and Photoflow for one minute, then rinsed in clean water, dipped in methanol and dried in hot air. The above procedure comprises one cycle. It may be necessary to repeat the above cycle several times before removing all the corrosion products. It was not possible to predetermine the exact number of cleaning cycles for any given specimen, since it depended upon the severity of the oxidation, roughness of surface, and the physical size of the sample. The specimen was observed optically after each cycle so that the process could be discontinued after the oxide or the corrosion product was removed and the specimen surface looked clean. After the specimen was thoroughly dried, it was either examined immediately, since it was subject to reoxidation at ambient atmosphere, or it was stored in a good desiccant awaiting examination.

The first plug specimen examined was from the area of the through hole "leaker" (Figure 24). Salient features of the surface were virtually nonexistent due to the erosive environment of the leaking secondary fluid. This particular specimen had visible copper colored deposits in evidence after electrolytic cleaning. These deposits were confirmed by EDS as copper, with zinc also in evidence (Figures 25a and 25b).

The second specimen examined (Figure 26) exhibited a transgranular fracture face with the "wood-like" appearance normally associated with progressive or fatigue-type fractures. Higher magnification scrutiny of the fracture face disclosed an area of possible fatigue interaction (Figures 27a-27d). The structure of low alloy steels makes a positive identification of fatigue striations extremely difficult. Area B of this fracture face (Figures 26) appears to be an area where the crack started to change its direction of growth, due to the effect of a dominant stress field, perhaps the vessel's hoop stress.

The third fracture face examined from the plug coupon (Figure 28) also displayed a fracture face characteristic of fatigue fractures. This particular fracture initiated at pits which were quite evident in the fractograph. Figure 29 is a fractograph of the same fracture surface, which clearly shows "beach marks" in evidence. These again are indicative of "fatigue-type" fractures.

The fracture faces associated with the three boat samples were also examined prior to electrolytic cleaning in order to ascertain any information regarding possible corrosive species which may have contributed to the failures.

All scans were performed near the leading edge of the cracks. The fracture faces exhibited normal iron and manganese, with traces of silicon and copper being the most prevalent additional constituents (Figures 30-32). With the exception of some scans having zinc or nickel present, these scans were typical of all scans on the fracture faces.

After electrolytic cleaning, the fracture faces for the three boat samples were examined. All three fractures exhibited transgranular features with the wood-like characteristics of fatigue fractures (Figures 33, 34 and 35). Additionally, the fractures had varying degrees of pitting associated with the initiation points of the fracture. An EDS scan of the area of initiation on fracture face MT indication 37/38 indicated Fe, Cr, Ni, Si, S, Cu and Zn (Figures 36, 37, and 37a).

Other pits were examined at the mouth of the cracks (Figures 38-40). Only the pit in Figure 38a exhibited additional elements present other than the typical ones of Fe, Mn, Ni, Cu and Zn. This pit also had present Al, Si, Cl and K. It is also interesting to note that the EDS analysis of the pit in Figure 40a had a difference in composition between the rim of the pit and the interior portion of the pit. The difference was evidenced by the element nickel not being present on the pit's rim but is present on the pit's interior surface.

VI. DISCUSSIONS/CONCLUSIONS

Indian Point-3 has operated on an all-volatile treatment from initial startup. This is one of only two units which has developed moderate to severe denting without a prior history of the phosphate treatment.

The Hudson River estuary at the Indian Point site ranges from fairly fresh water to a brackish environment, depending on the season. Copper alloys in the condenser tubes at the site have been corroded by this in-leaking brackish water so that the sludge analysis in Indian Point-3 shows concentrations of copper as high as 45% and iron 40%. A significant amount of Cl^- is present as well. Analysis of this sludge has shown significant quantities of copper as cuprous oxide (Cu_2O) and is also the only plant that contains significant amounts of alpha hematite (alpha-Fe_2O_3) in the sludge pile. The presence of both of these constituents indicates that oxygen control in the Indian Point-3 steam generators has been poor for a considerable period of time. The aforementioned poor oxygen control, plus the fact that hydrazine levels have been kept low in the steam generators (due to environmental concerns), have definitely contributed to the pitting of the shell material.

Additionally, in January 1981, the unit suffered a turbine blade failure which damaged approximately 50 condenser tubes and allowed chloride into the steam generators with recorded levels of up to 325 parts per million (ppm). This chloride intrusion may have had a decided influence on initiating pits at the inside surface of the steam generator shell.

Steam generators have had thermal fatigue indicated as the causative factor in other failures, such as cracking of feedwater nozzles [1]. These nozzle cracks showed large numbers of crack arrests and beach marks, suggesting that their propagation was also discontinuous in nature and caused by a stress mode that was cyclic in nature. The conclusions on the failure mechanism of these nozzles was low cycle corrosion fatigue. It is interesting to note that in the case of the feedwater nozzle cracking, machining marks played a role in the initiation of the cracks since they formed sites for localized corrosion (pits). The cracks observed on this investigation were quite similar in appearance to the feedwater cracks (by optical and electron microscopy).

Constant Extension Rate Tests (CERT) performed on A508 Cl 2 steel [2] (another pressure vessel steel) in oxygenated water at higher temperatures have demonstrated that this particular steel is susceptible to transgranular stress corrosion cracking in pure water between 100°C to 288°C if the water contains 1 or 8 ppm oxygen. This work also described pitting corrosion occurring in pure water (of the same oxygen content) at 100°C and 150°C. Transgranular cracks nucleating from the corrosion pits were also noted.

A recent EPRI report [3] on environment concerns for carbon steel piping concluded that carbon steel is susceptible to environmental assisted cracking in high temperature oxygenated water environments, especially under high amplitude, low frequency cyclic loading. Low frequency cyclic stresses would be the type encountered during steam generator operation.

Oxygen has been considered to be a strong influencing factor in the general corrosion of carbon steels in nuclear reactor environments [4]. Oxygen content has also been shown to exert considerable control on the incubation time of crack growth in A302 Grade B material [5,6] subjected to corrosion fatigue testing. These results stemmed from a testing program initiated after the Japanese Power Demonstration Reactor developed cracks in its stainless steel overlay which propagated into the A302 Grade B base material.

The nucleation of the pits on the shell walls was probably the combined effect of oxygen with the copper species promoting a more oxidizing potential in solution. The effect of chlorides [7,8] in promoting pits in iron has been investigated and probably aided in pit nucleation. Carbon steel has also been known to be susceptible to cracking by chloride solutions at 316°C [9].

Although residual stresses and their relative importance in fatigue life have been argued extensively [10,11,12], it is generally accepted that fatigue strength increases when specimens tested have compressive residual stresses. If a weld has received an insufficient or inadequate stress relief, the stresses present would more than likely be of the tensile rather than compressive variety in the weld. Another characteristic of fatigue is that many fatigue failures are the result of material stress raisers on a free surface. Pits on the inside surface of a pressure vessel are effective stress raisers.

The aforementioned discussion and previous observations have led to the following conclusions regarding the cracking of the Indian Point 3 steam generators:

1) All of the cracks examined were transgranular in nature and were associated with pits on the inside surface of the steam generators.

2) The hardness measurements after heat treatment and on the "as received" material indicate the possibility of high residual stresses associated with the welds. These hardness values were not excessive, however.

3) The relatively high O_2 levels and the copper species in solution contributed to the pitting on the inside surface of the vessels. The previous chloride intrusion may also have complemented this effect.

4) The observation of "beach marks" and possible fatigue striations, coupled with the transgranularity of the cracks, is characteristic of a low cycle corrosion fatigue phenomenon.

5) Although corrosion fatigue is considered the primary cause of degradation, the relative importance of corrosion in the crack propagation rate is currently undetermined. The possibility of stress corrosion cracking being a contributing cause of the failure cannot be entirely discounted due to the lack of literature concerning this alloy's response in copper containing oxygenated water.

VII. ACKNOWLEDGEMENTS

The author wishes to thank R. Sabatini for the SEM/EDS work, L. Gerlach for his able assistance in testing, A. Cendrowski and D. Horn for the hardness measurements, D. Thompson for her typing skills, and Dr. J. R. Weeks for his continued support.

VIII. REFERENCES

1. Vyas, B., Czajkowski, C. J. and Weeks, J. R., Nuclear Technology, 55, (November 1981).

2. Choi, H., Beck, F. H., Szklarska-Smialowska, Z. and MacDonald, D. D., Corrosion, 38, No. 3, (March 1982).

3. Weinstein, D., EPRI NP-2406, Project 1248-1, Final Report, (May 1982).

4. Pearl, W. L. and Wazadlo, G. P., Corrosion, 21, (August 1965).

5. Kondo, T., Kikuyama, T., Nakajima, H., Shindo, M. and Nagasaki, R., Proceedings: Corrosion Fatigue: Chemistry, Mechanics and Microstructure, (June 1971) (NACE)

6. Kondo, T., Nakajima, H. and Nagasaki, R., Nuclear Engineering & Design, 16, (1971).

7. Janik-Czachor, M., Wood, G. C. and Thompson, G. E., Br. Corros. J., 15, No. 4, (1980).

8. Szauer, T. and Jakobs, J., Corrosion Sc., 16, (1976).

9. Strauss, M. B. and Bloom, M. C., Corrosion, 553t-556t (May 1961).

10. Welding Handbook, Volume 1, 7th Edition.

11. Mechanical Metallurgy, 2nd Edition, G. E. Dieter, ed., McGraw Hill (1976).

12. Physical Metallurgy Principles, R. E. Reed-Hill, ed., D. Van Nostrand Co., (1964).

TABLE 1

Chemical and Tensile Properties of A302 Grade B Steel

Chemical Requirements

Elements	Composition, %
Carbon, max*:	
Up to 1 in. (25 mm) incl. in thickness	0.20
Over 1 to 2 in. (50 mm) incl.	0.23
Over 2 in. in thickness	0.25
Manganese:	
Heat analysis	1.15-1.50
Product analysis	1.07-1.62
Phosphorus, max*	0.035
Sulfur, max*	0.040
Silicon:	
Heat analysis	0.15-0.40
Product analysis	0.13-0.45
Molybdenum:	
Heat analysis	0.45-0.60
Product analysis	0.41-0.64
Nickel:	
Heat analysis	--
Product analysis	--

*Applies to both heat and product analyses

Tensile Requirements

Tensile Strength, ksi (MPa)	80-100 (550-690)
Yield Strength, min, ksi (MPa)	50 (345)
Elongation in 8 in. or 200 mm. min. %	15*
Elongation in 2 in. or 50 mm. min. %	18*

*See Specification ASTM A20

TABLE 2

Chemical and Mechanical Properties of E8018 C-3 Welding Electrode

Chemical Requirements	Percent*
Carbon	0.12
Manganese	0.40-1.25
Phosphorus	0.030
Sulfur	0.030
Silicon	0.80
Nickel	0.80-1.10
Chromium	0.15
Molybdenum	0.35
Vanadium	0.05

*Single values are maximum percentages

Mechanical Requirements	
Tensile Strength, min, psi	80,000
Yield Strength @ 0.2% offset, psi	68,000-80,000
Elongation in 2 in., min, percent	24

TABLE 3

Hardness Readings of Plug Sample

As Received (KHN Values/500 gm)

Base Metal			HAZ			Weld
248	296	240	323	267	287	311
259	289	243	342	280	280	280
251	282	246	332	281	289	278
248	307	247	367	280	295	280
247	278	246	356	284	292	
245	269	244	298	303	366	
			365			

After 1000°F Heat Treatment (KHN Values/500 gm)

Base Metal			HAZ			Weld
231	264	280	314	295	282	247
244	263	264	346	296	316	232
226	267	274	328	311	311	243
238	263	270	314	295	322	237
228	258	288	284	291	321	235

After 1125°F Heat Treatment (KHN Values/500 gm)

Base Metal			HAZ			Weld
229	210	279	280	269	262	231
220	213	274	291	246	280	221
224	221	282	288	279	267	237
221	220	284	277	267	265	234
217	215	280	295	262	248	221

TABLE 3 (Cont'd)

Rockwell Hardness Values (R_B unless noted)

As Received

Base Metal		HAZ		Weld	
90.5	94	97	43.5(R_D)	96.5	99.5
92.5	92.5	43.5(R_D)	96	96.5	92.5
92.5	93	46.5(R_D)	44.5(R_D)	95.5	92
92.5	95	99.5	50(R_D)	97	91.5
93		41(R_D)		98	

After 1000°F Heat Treatment (R_B unless noted)

Base Metal		HAZ		Weld	
90	95.5	98	42(R_D)	97	98
92	91	43.5(R_D)	41(R_D)	95	95
93	93	48(R_D)	47(R_D)	98	92
94.5	93	97	43(R_D)	97	95
95		40(R_D)		96.5	

After 1125°F Heat Treatment (R_B unless noted)

Base Metal		HAZ		Weld	
93	92	100	41(R_D)	97	97
93	92	43(R_D)	100	96	96
93	93	42(R_D)	41(R_D)	97	96
92	92	97	40(R_D)	96	95
92		40(R_D)		95	

TABLE 4

Hardness Readings of Boat Samples
(As Received)

Sample 37/38

Base Metal		HAZ		Weld	
227	220	324	312	300	255
228	240	307	307	281	264
229		303	373		
		396	357		

Sample 44

Base Metal		HAZ		Weld	
274	272	252	320	267	261
274	261	338	324	264	255
255		329		246	

Sample 46
Only one microstructure noted

227	229	240	235	219
233	233	233	237	240

GRAPH #1

A Graphical Comparison of the Hardness Values
of the BASE METAL After Heat Treatment

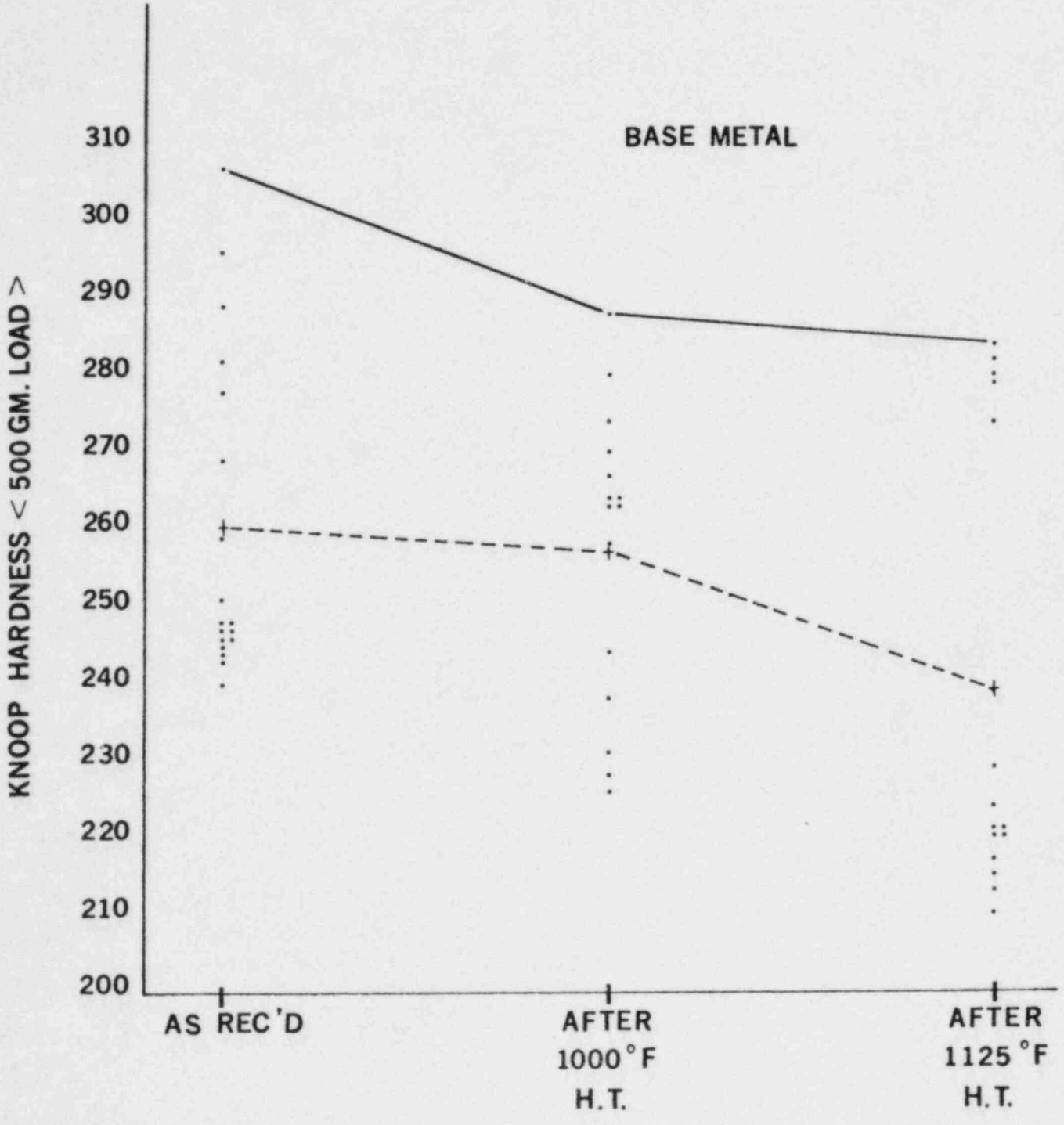

—— = Maximum Hardness Values

--- = Average Hardness Values

GRAPH #2

A Graphical Comparison of the Hardness Values
of the WELD METAL After Heat Treatment

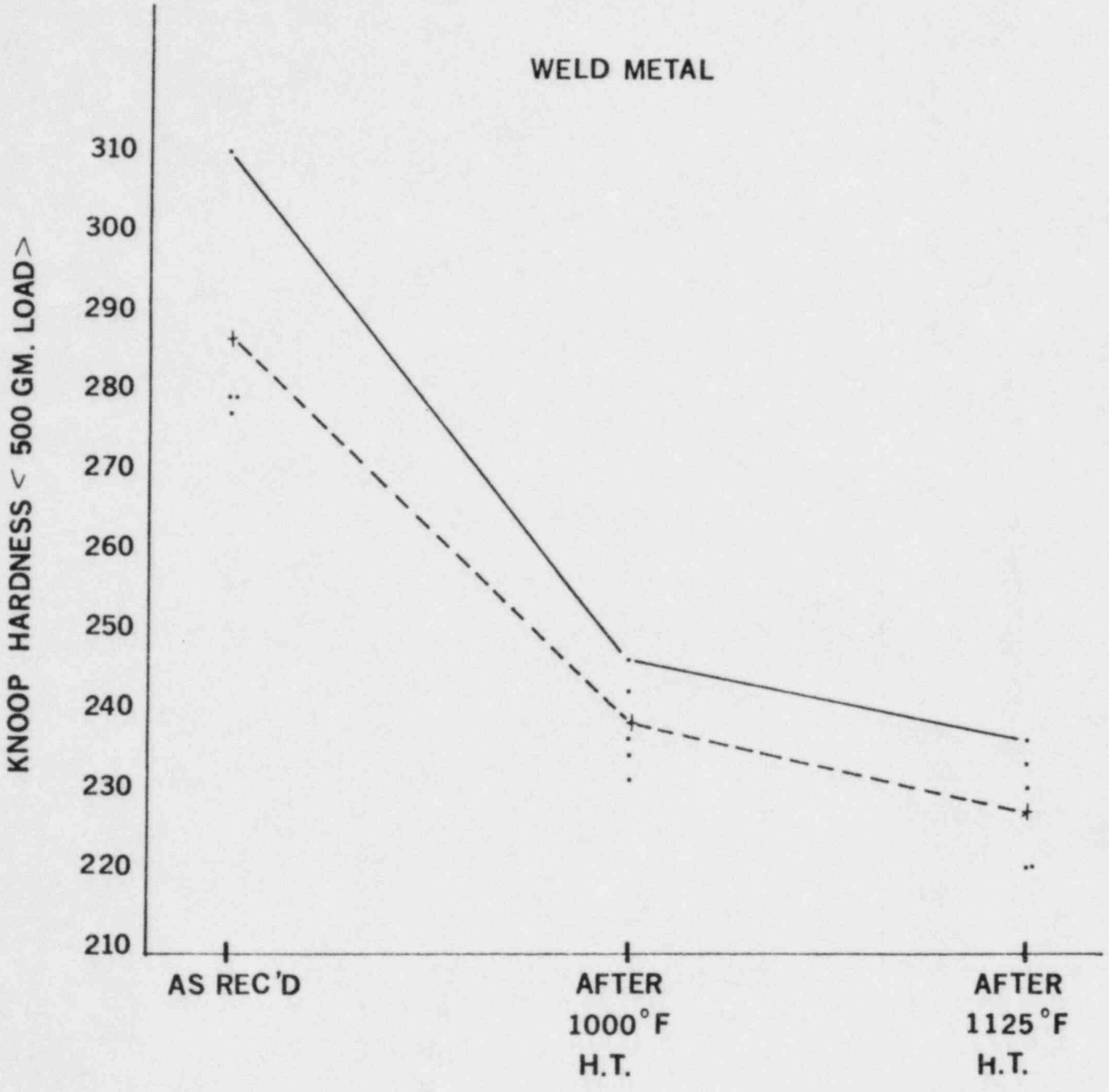

—— = Maximum Hardness Values

--- = Average Hardness Values

GRAPH #3

A Graphical Comparison of the Hardness Values
of the HEAT AFFECTED ZONE After Heat Treatment

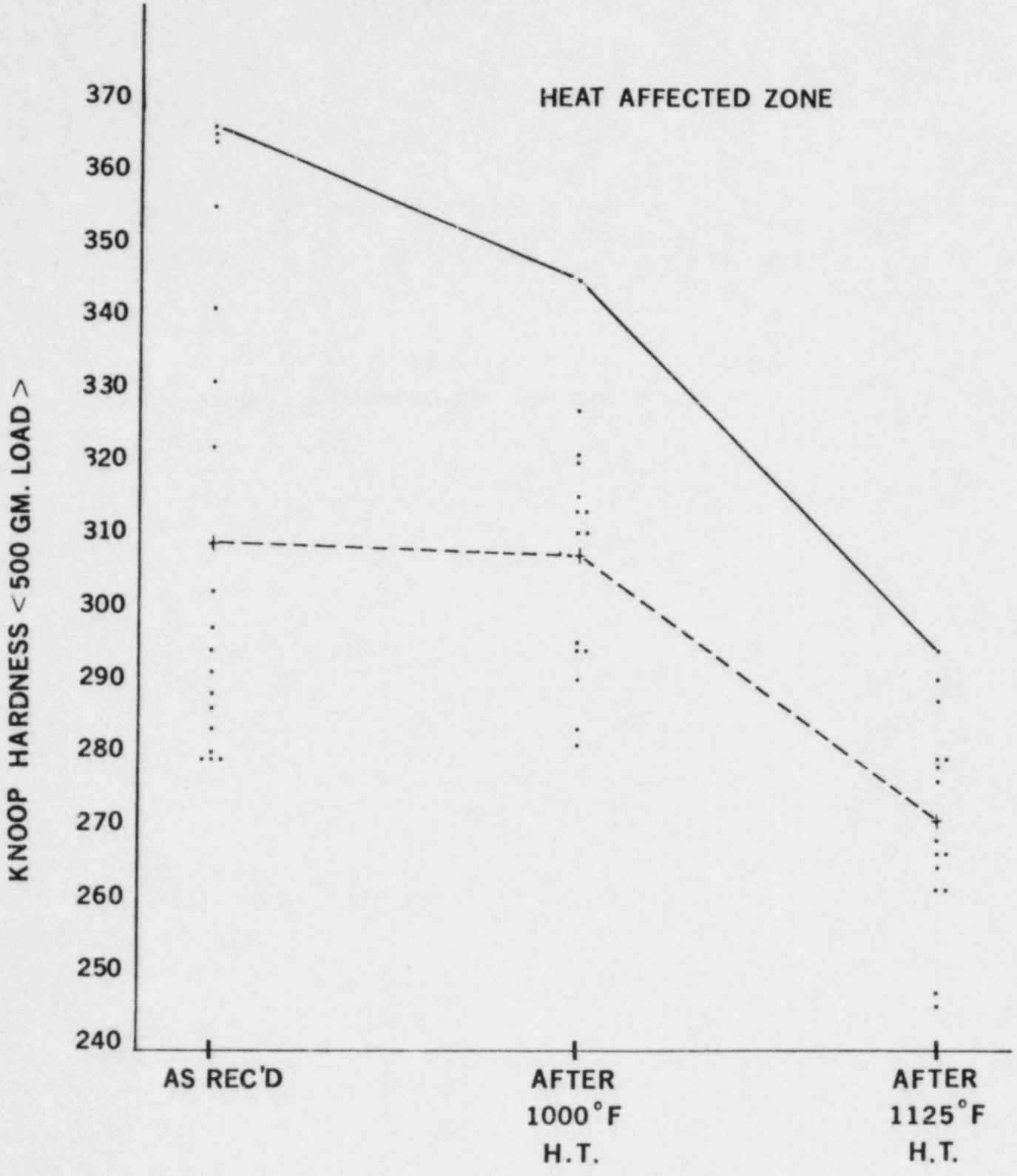

—— = Maximum Hardness Values

--- = Average Hardness Values

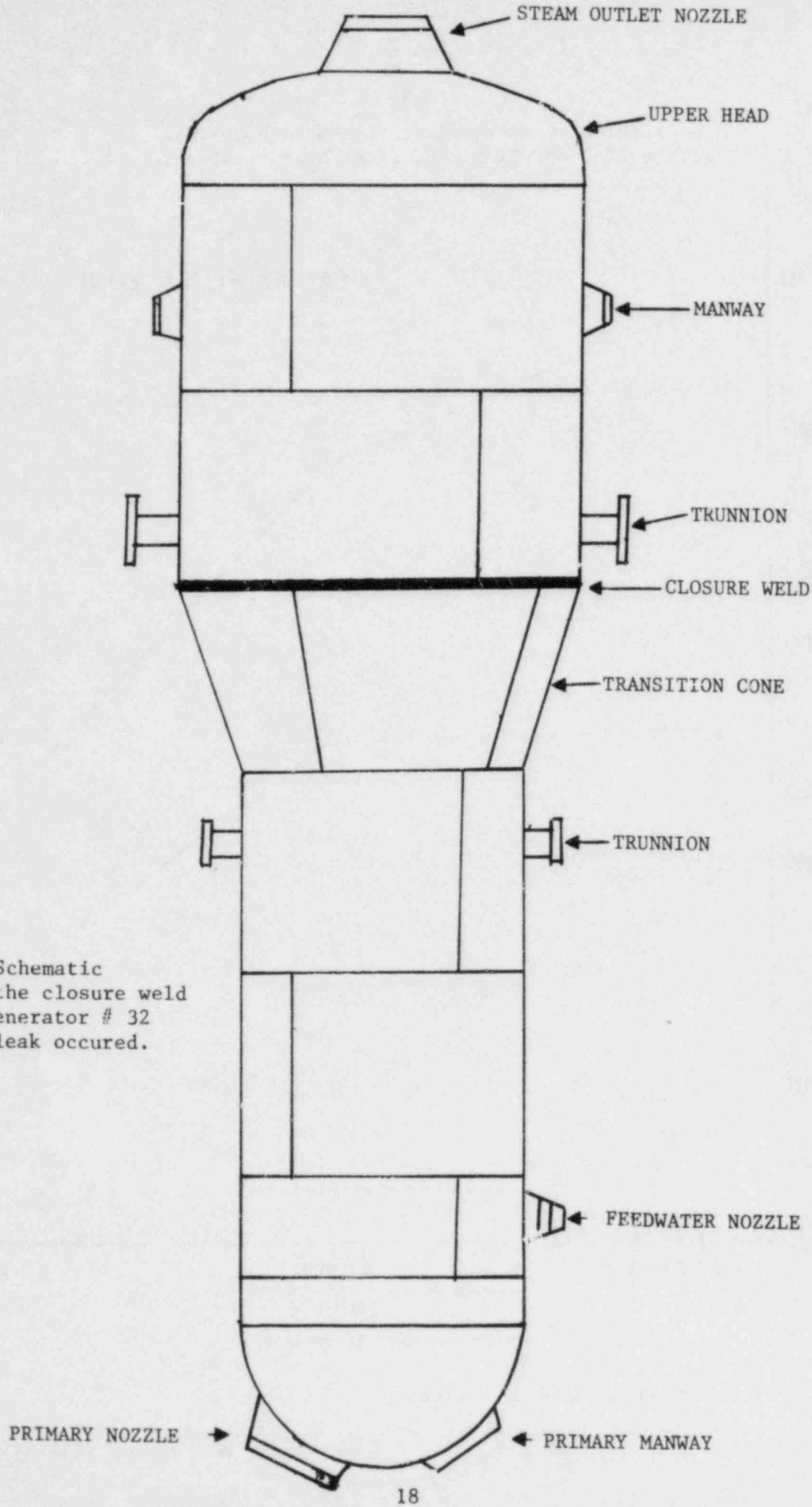

Figure 1. Schematic depicting the closure weld of Steam Generator # 32 where the leak occured.

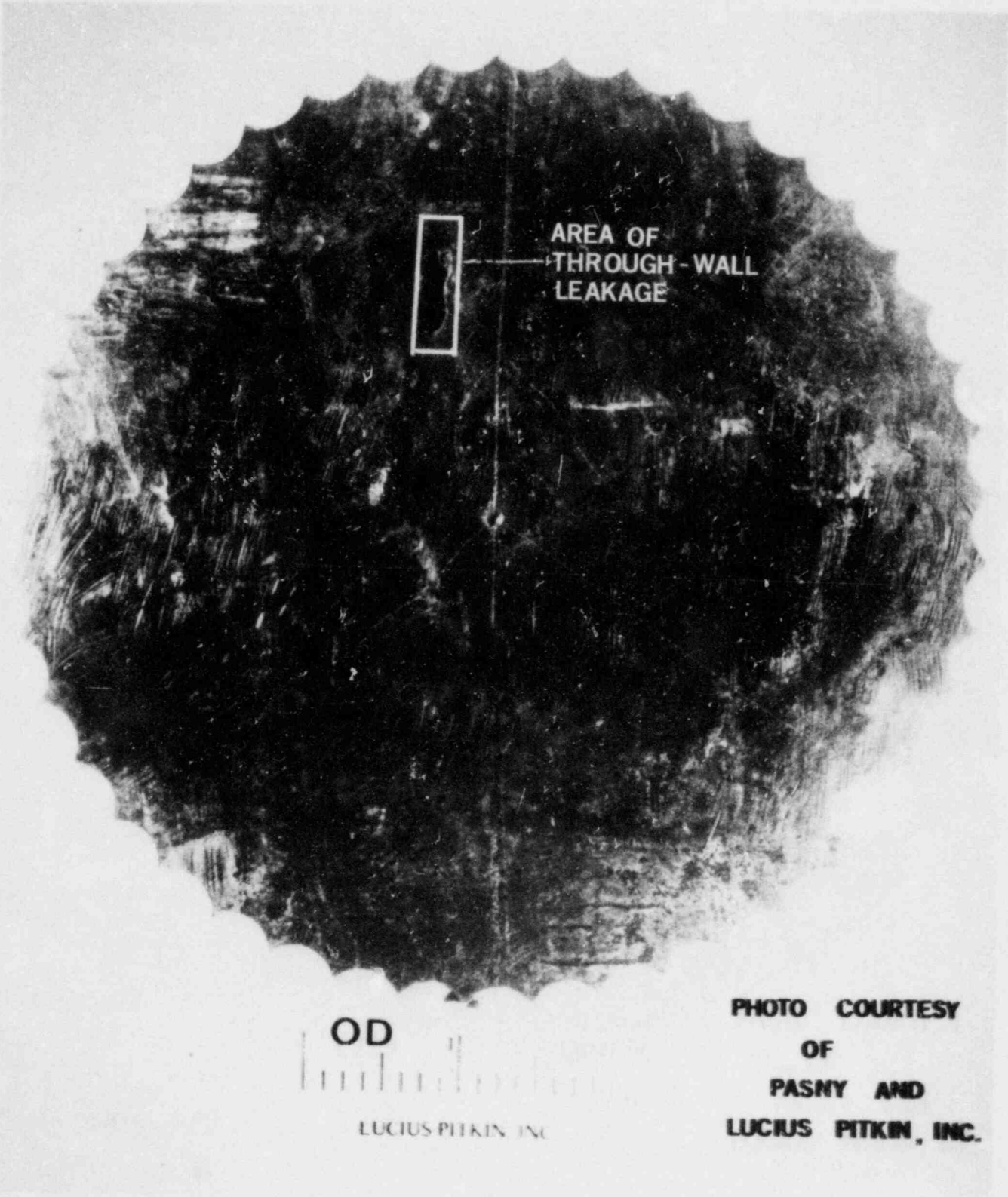

Figure 2. Photograph of 6" plug removed
from steam generator #32
showing the through wall "leaker"

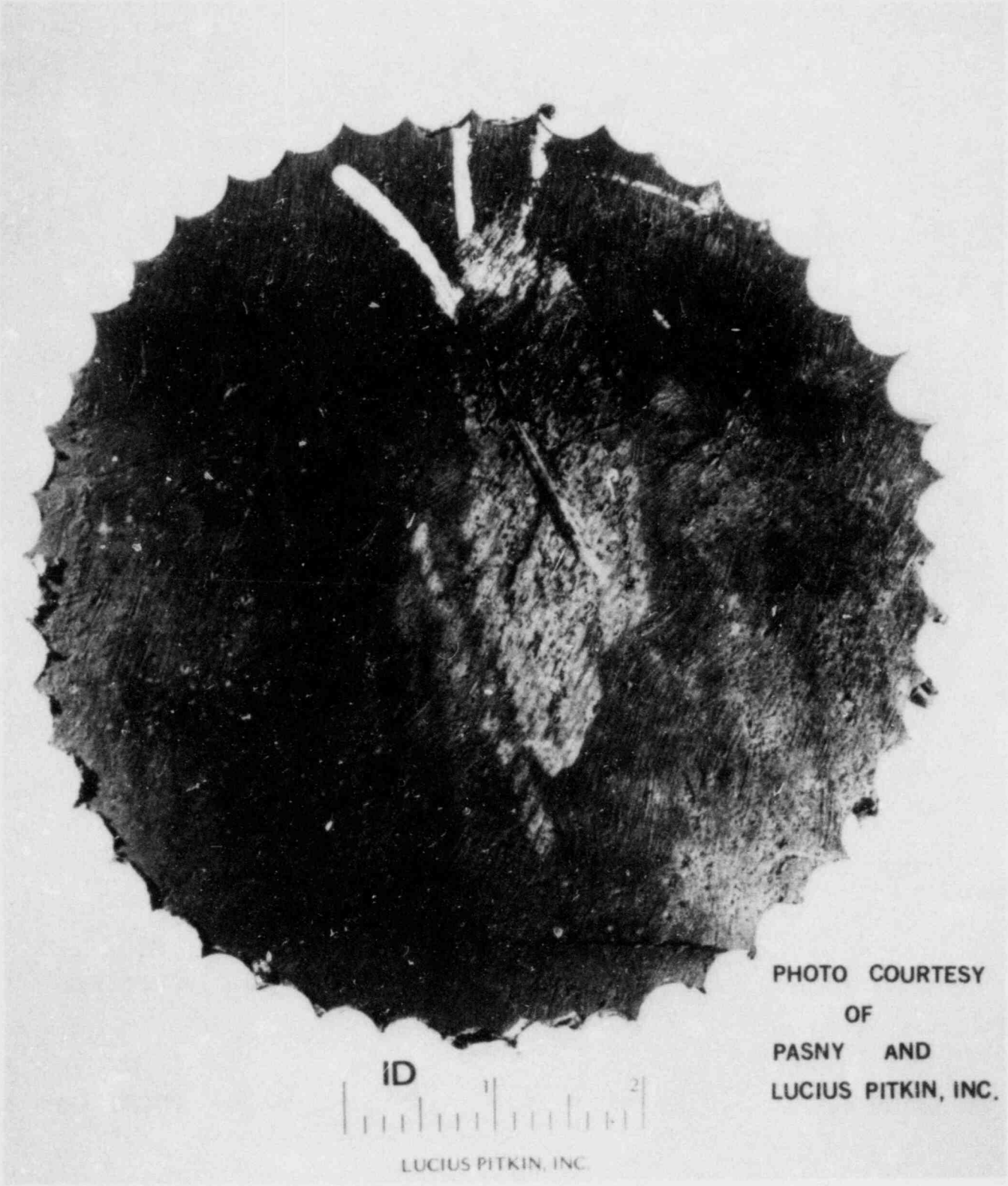

Figure 3. Photograph of the inside surface of steam generator #32 showing cracks and evidence of pitting.

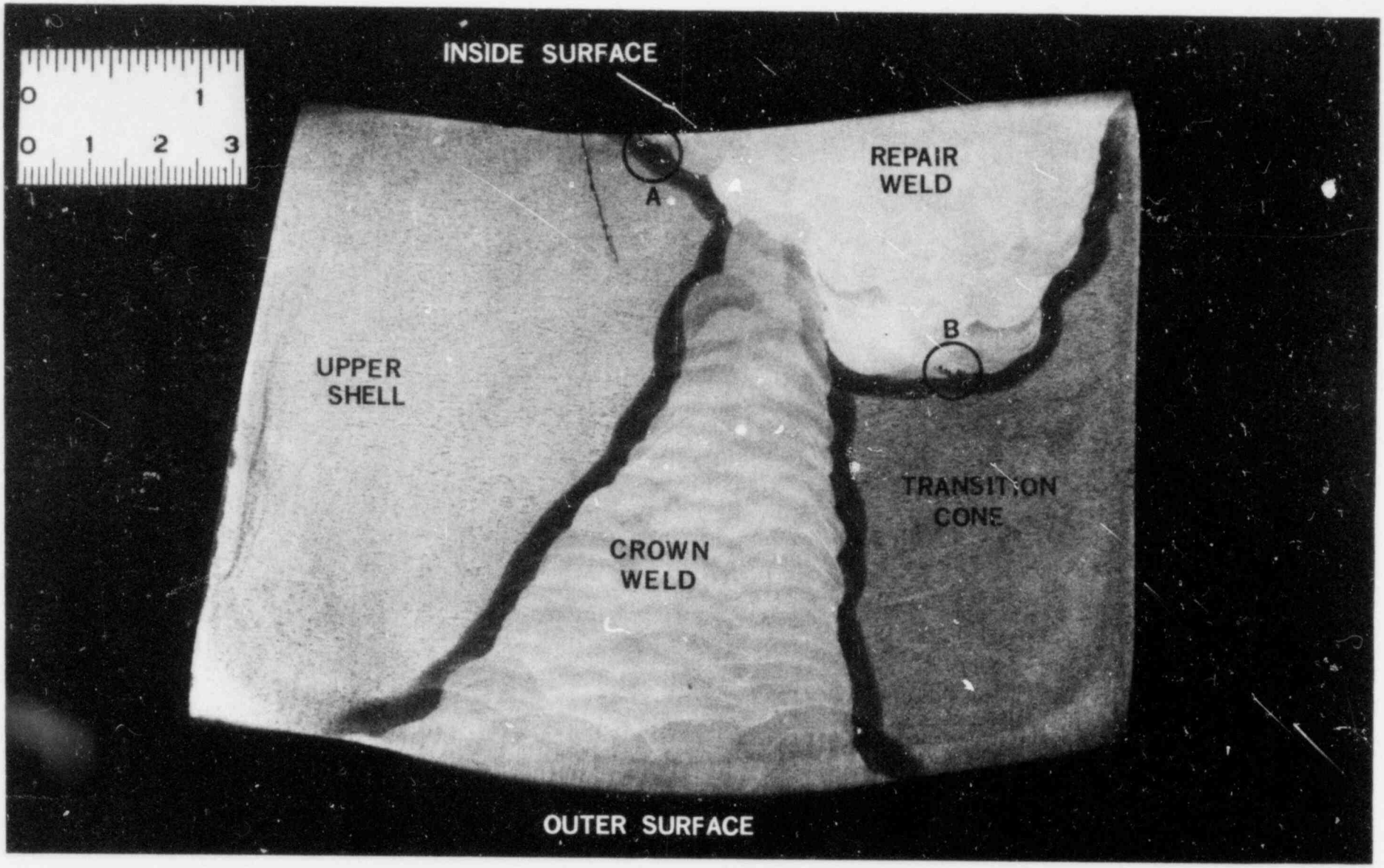

Figure 4. Photograph of a cross-section of the 6" plug after etching. Evident in the photograph is the relative position of the crack to the weld.Additional areas of interest include Area A- a region of lack of fusion and Area B- a region of porosity.

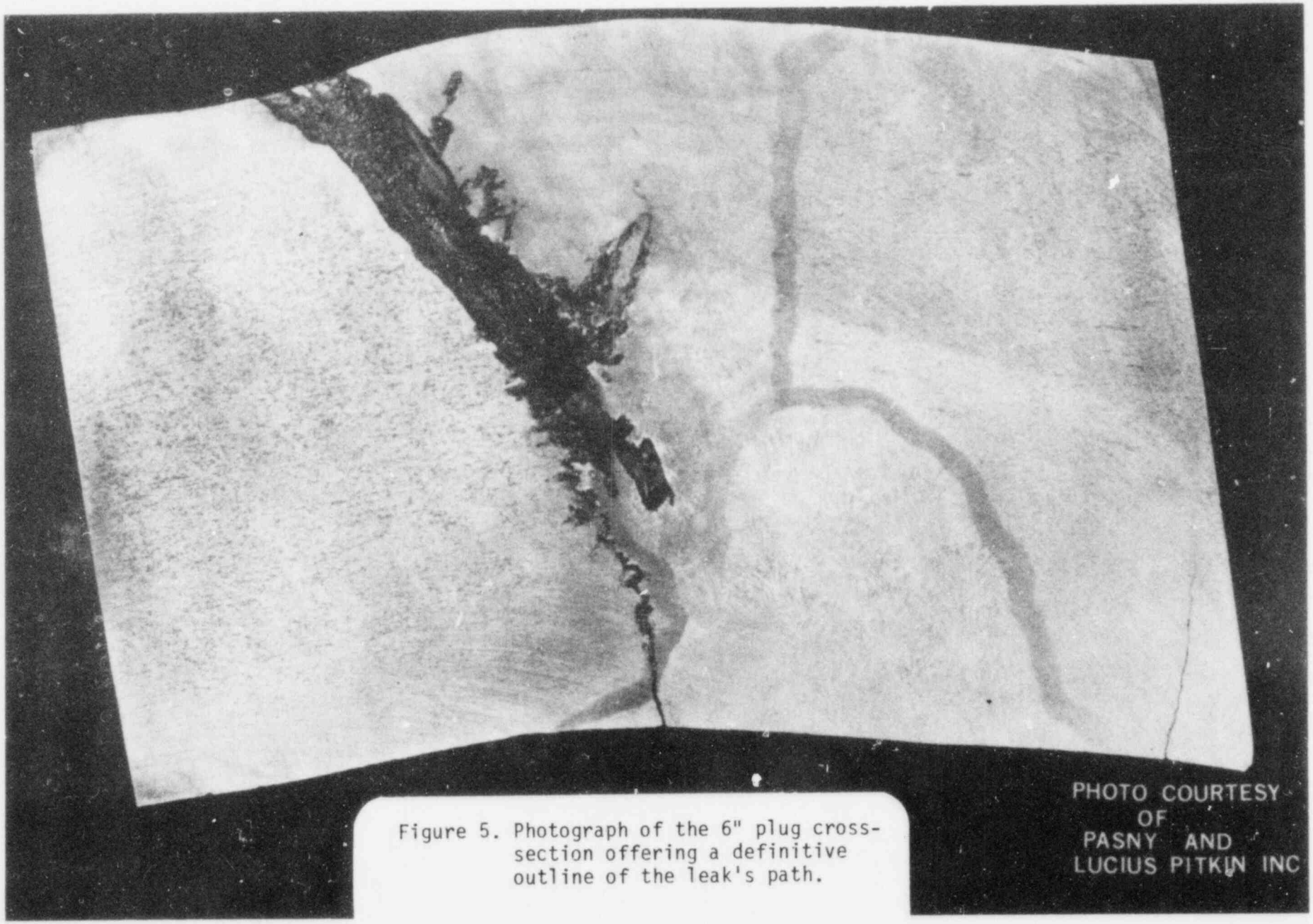

Figure 5. Photograph of the 6" plug cross-section offering a definitive outline of the leak's path.

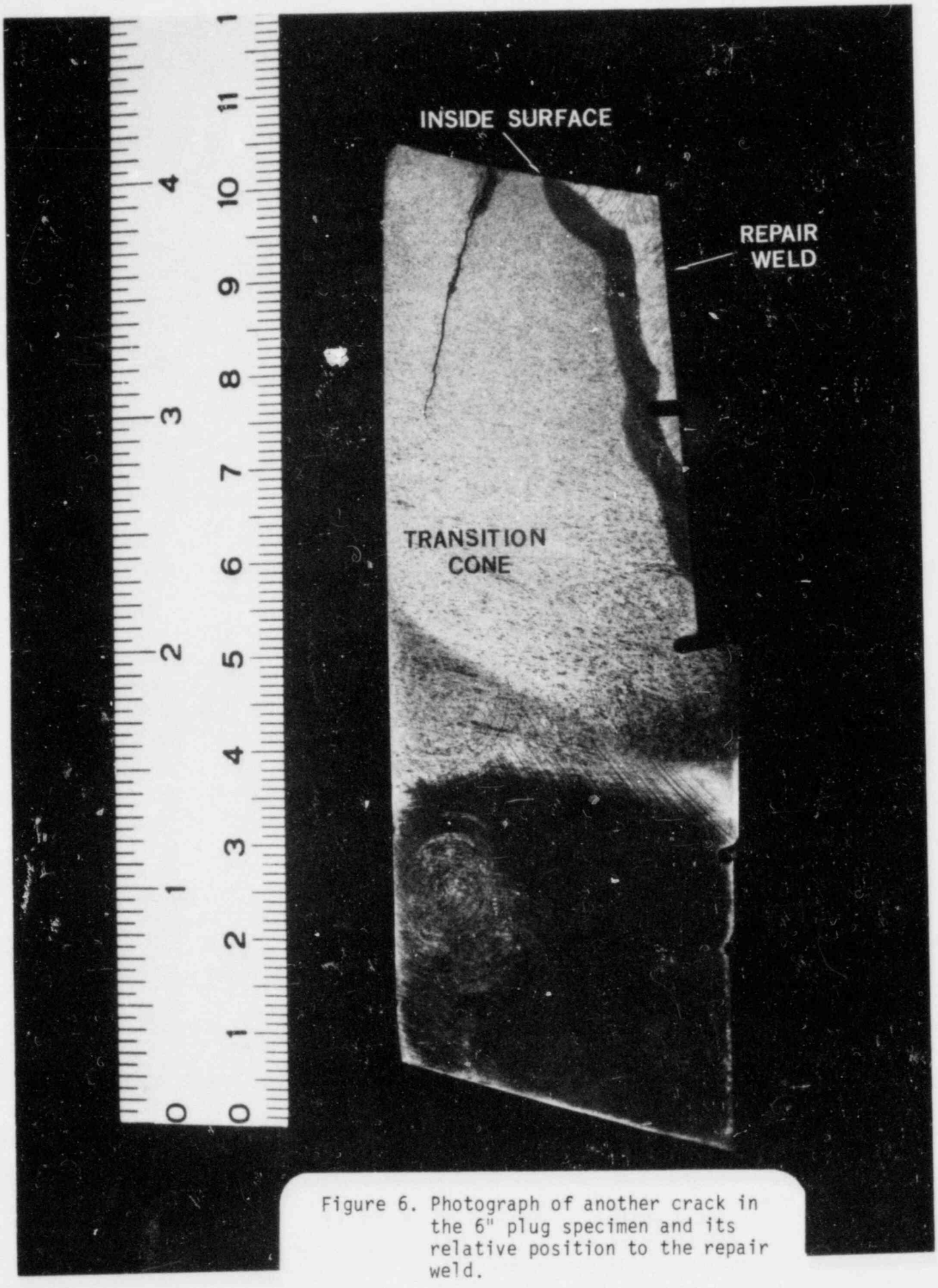

Figure 6. Photograph of another crack in the 6" plug specimen and its relative position to the repair weld.

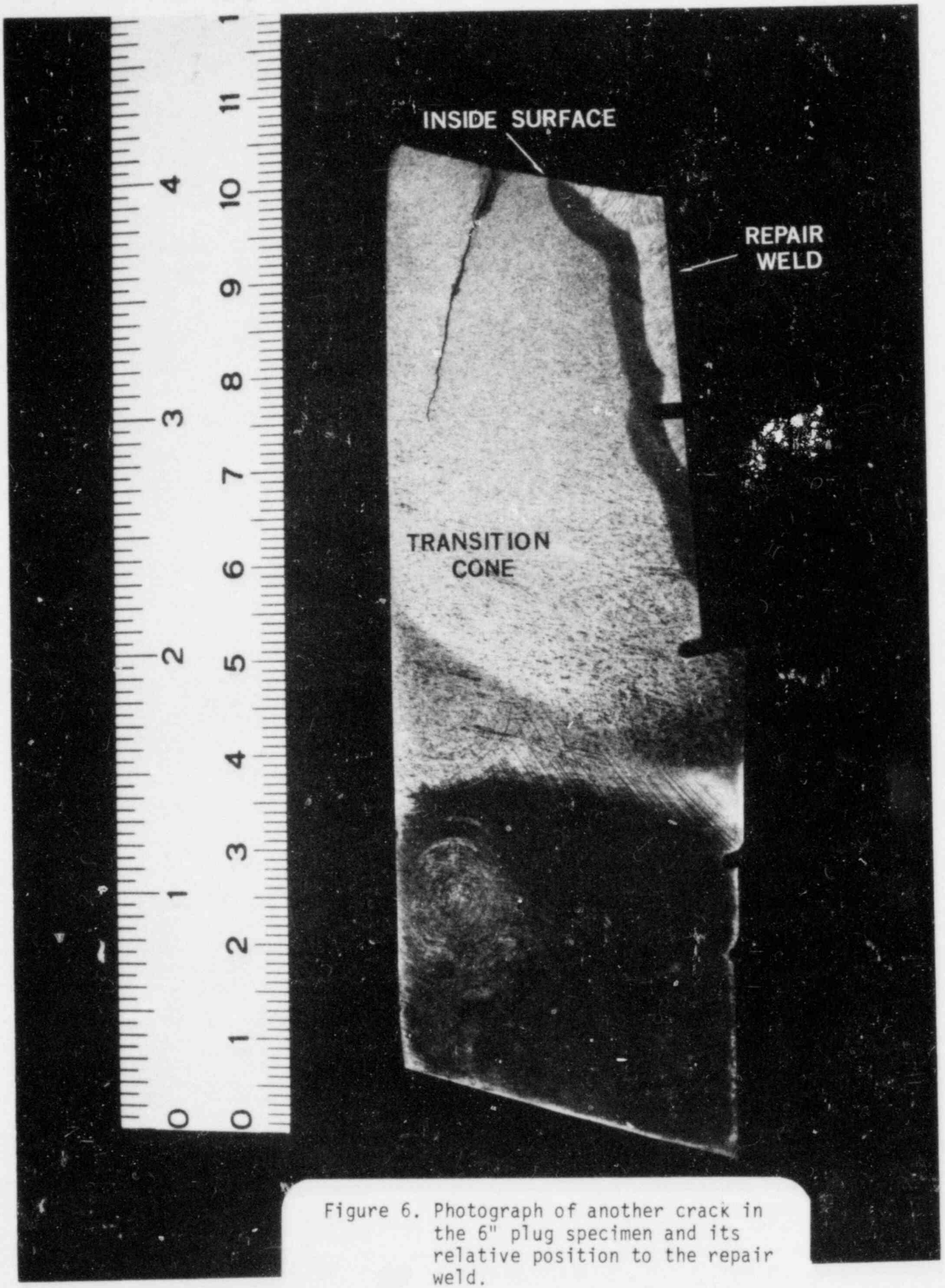

Figure 6. Photograph of another crack in the 6" plug specimen and its relative position to the repair weld.

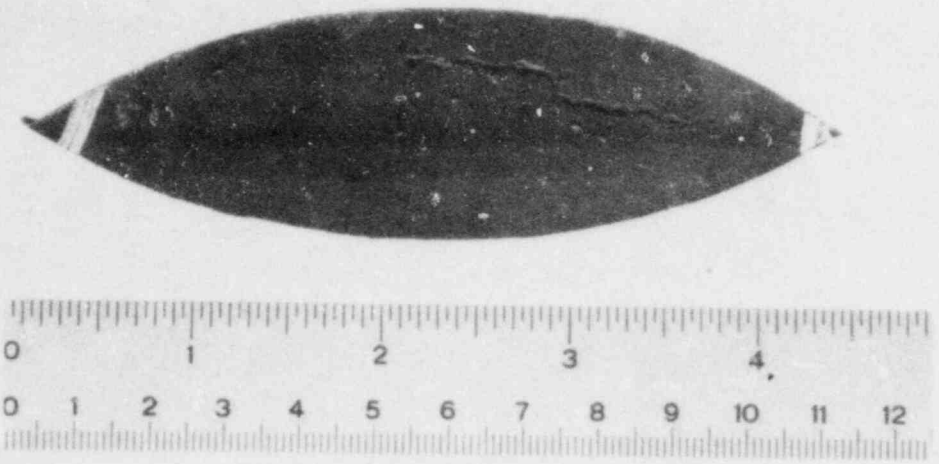

Figure 7. Photograph of the top side (inside surface) of the boat sample MT #44 .

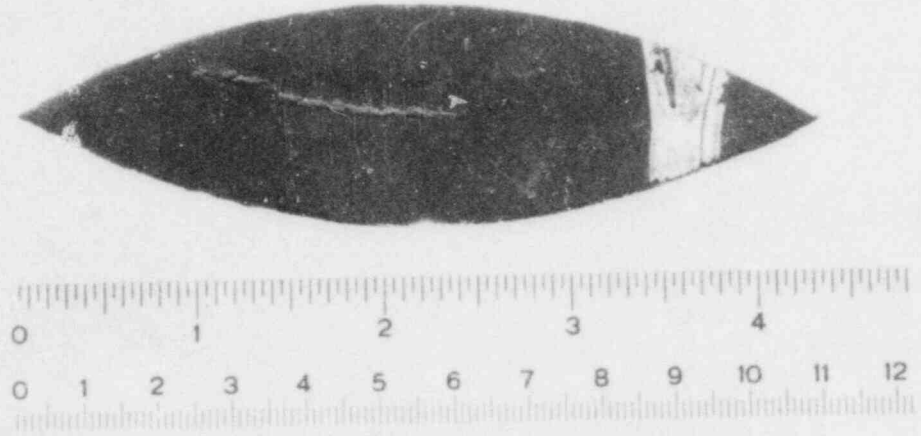

Figure 8. Photograph of the top side of boat sample MT #46.

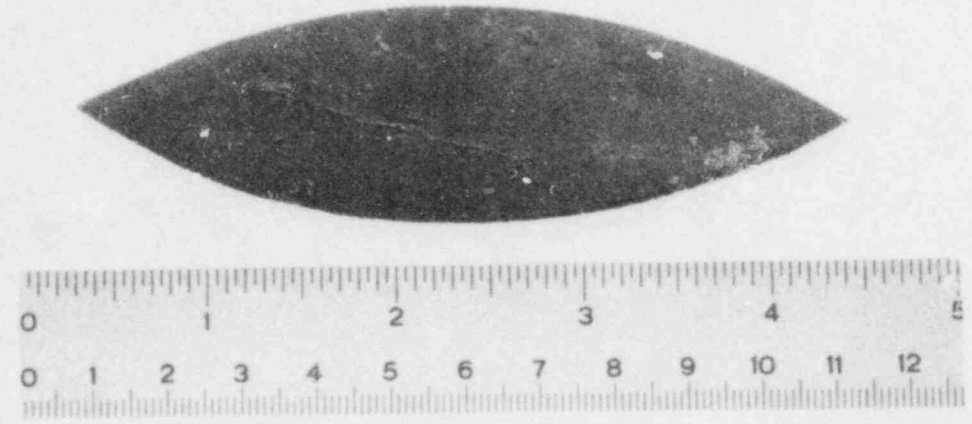

Figure 9. Photograph of the top side of boat sample MT #37,38. Note the extensive pitting .

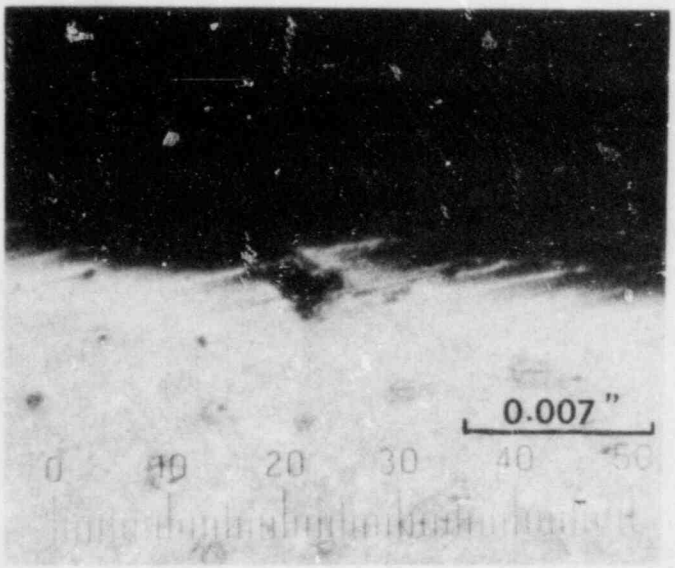

150X

Figure 10. Optical photomicrograph of one of the pits seen with no crack associated with it.

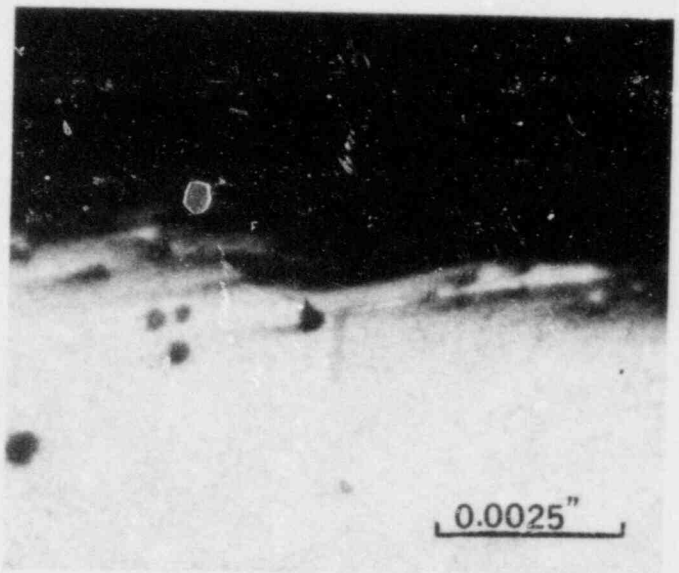

400X

Figure 11. Optical photomicrograph of a shallow pit with a transgranular crack at the bottom of the pit.

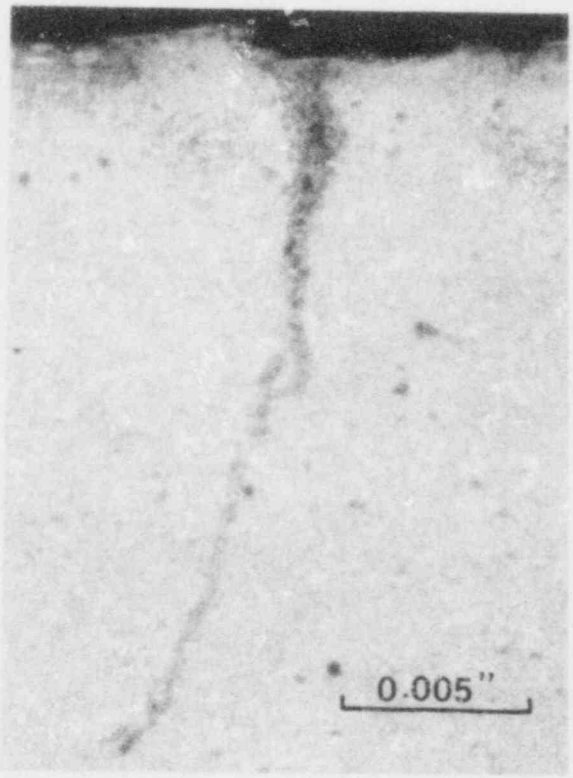

200X

Figure 12. Photomicrograph of another transgranular crack. Note the lack of branching.

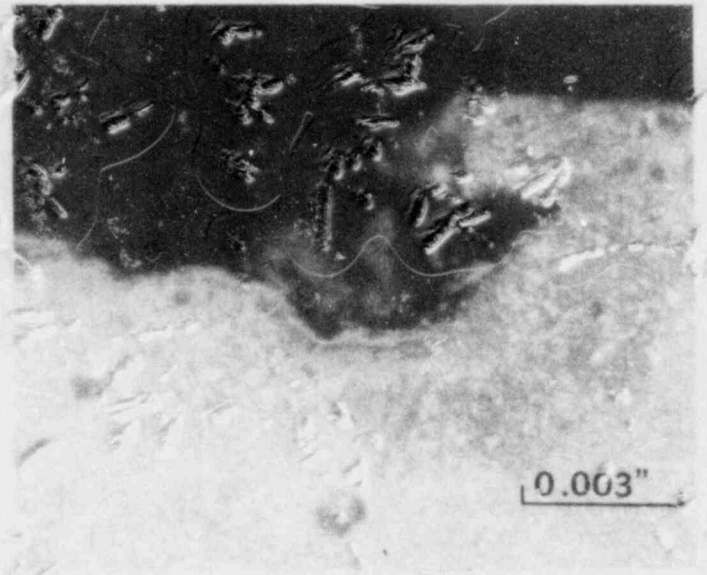

250X

Figure 13. Photomicrograph of one of the shallow, open-mouthed cracks at the bottom of a pit.

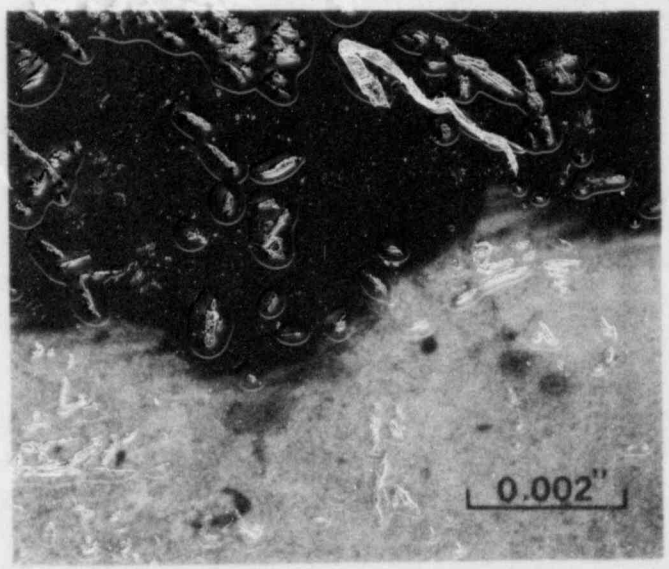

400X

Figure 14. Another smaller crack found at the bottom of a pit.

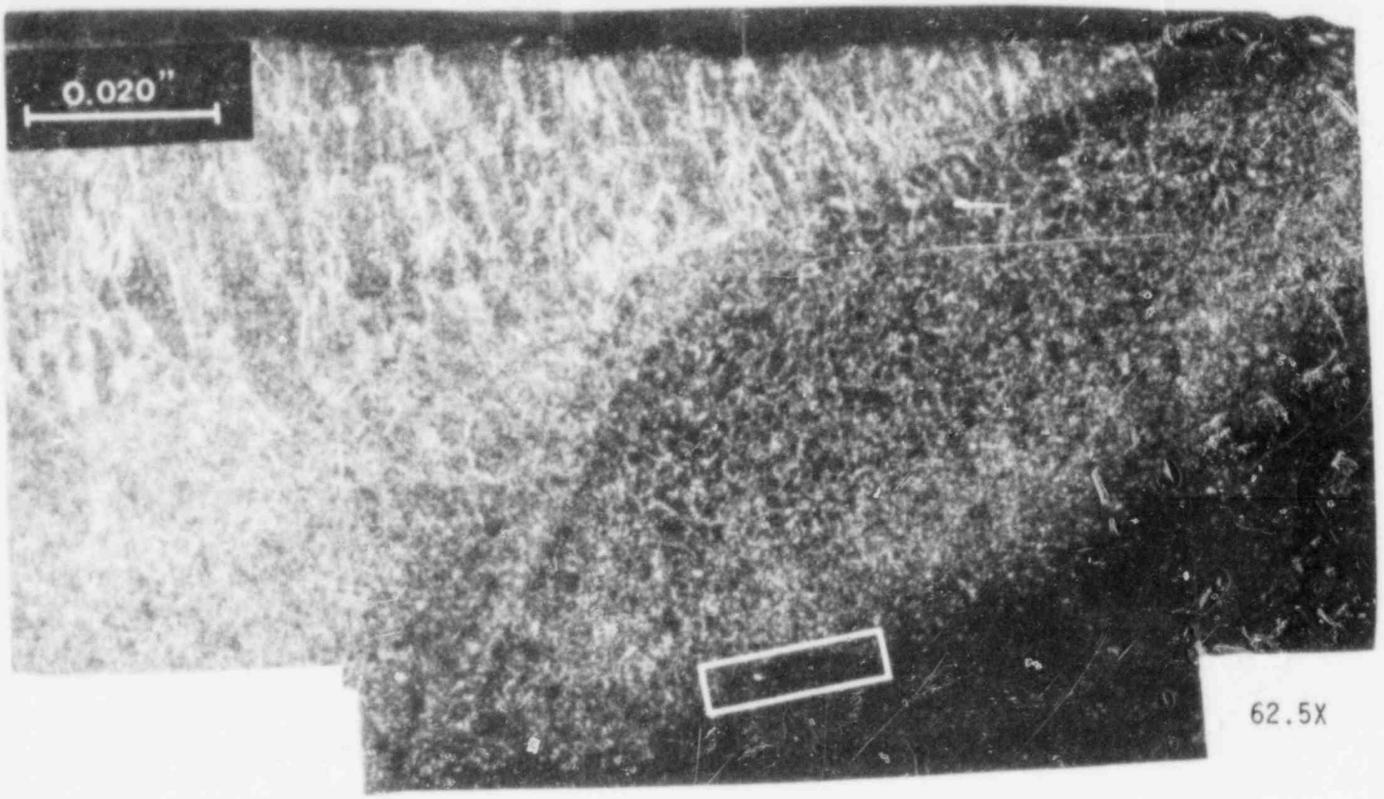

Figure 15. Photomicrograph depicting the area of "lack of fusion" shown in Figure 4 (Area - A).

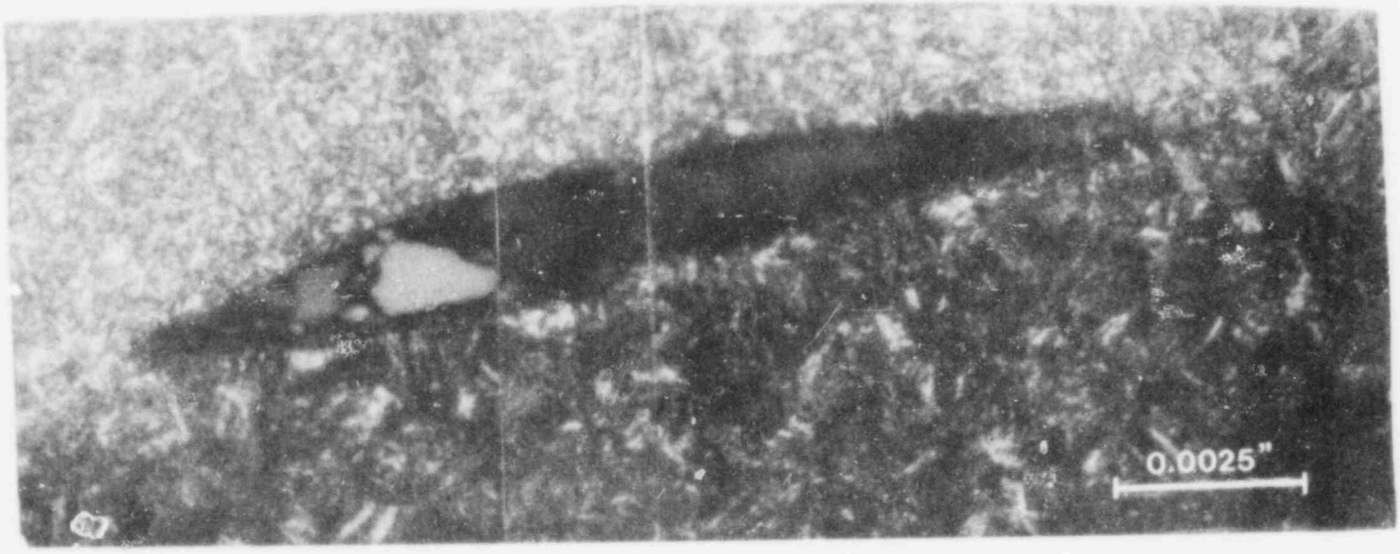

400X

Figure 16. Higher magnification photomicrograph of the area of "lack of fusion" showing blunted ends and no additional cracking evident.

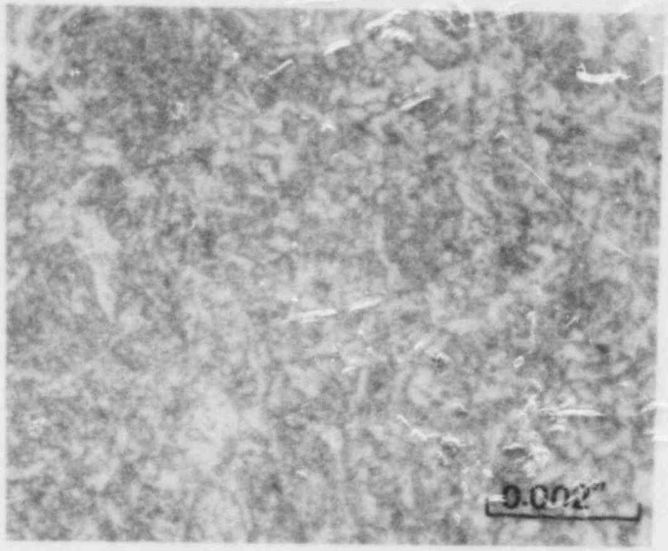

400X

Figure 17. Photomicrograph depicting the base metal's structure as a tempered martensite.

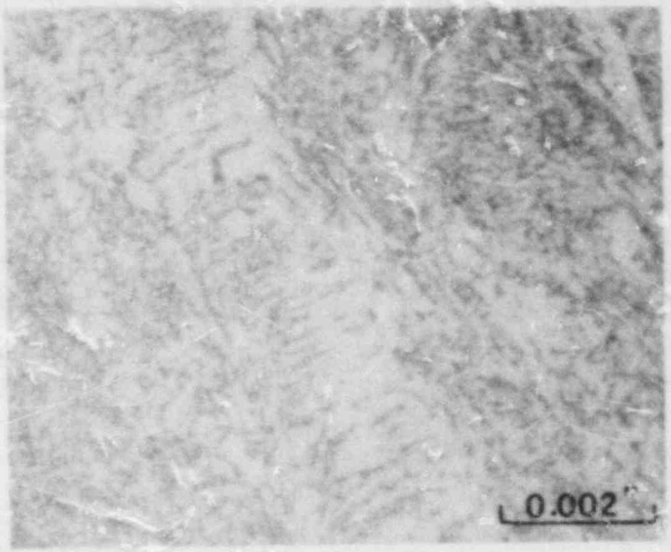

400X

Figure 18. Photomicrograph of the weld metal , showing a characteristic dendritic structure.

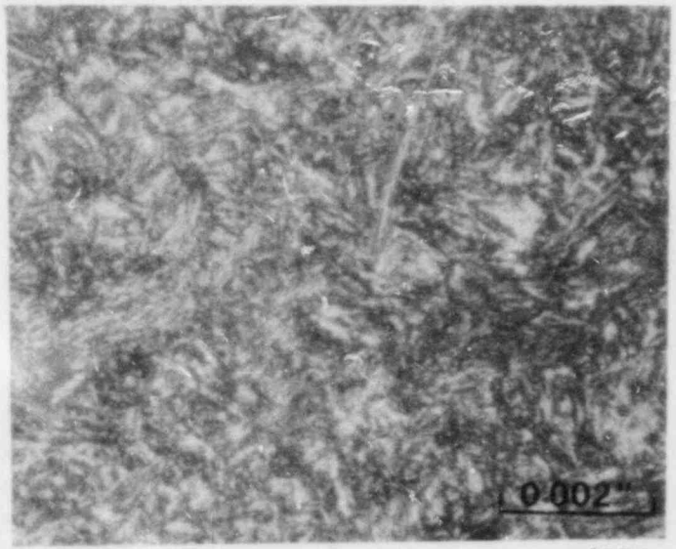

400X

Figure 19. Photomicrograph of the 6" plug's heat affected zone -hard martensite.

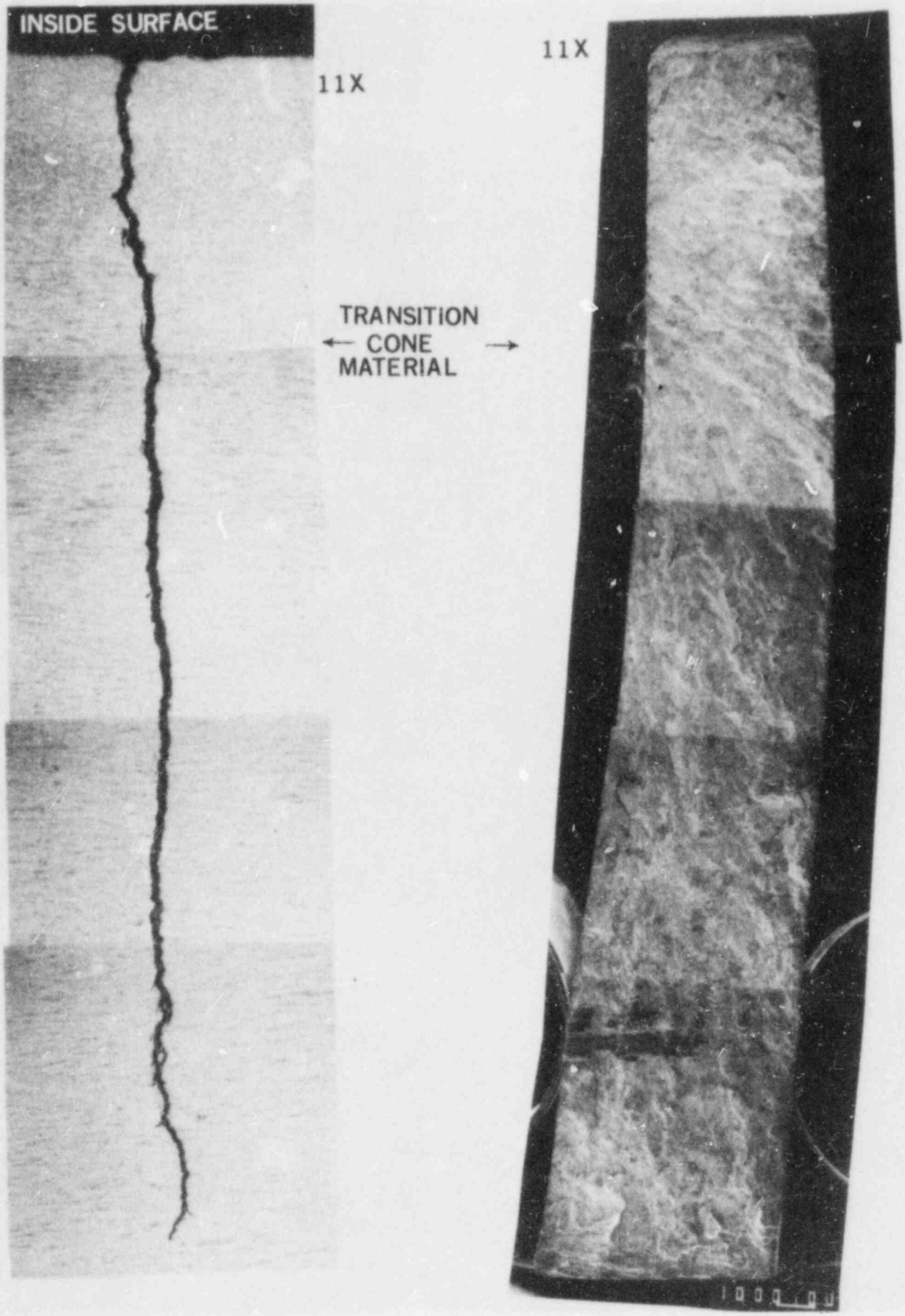

Figure 20. A comparison between the optical photomicrograph and the fractograph of the crack shown in Figure 6.There is virtually no crack branching evident. Note the discontinuous nature of the fractograph.

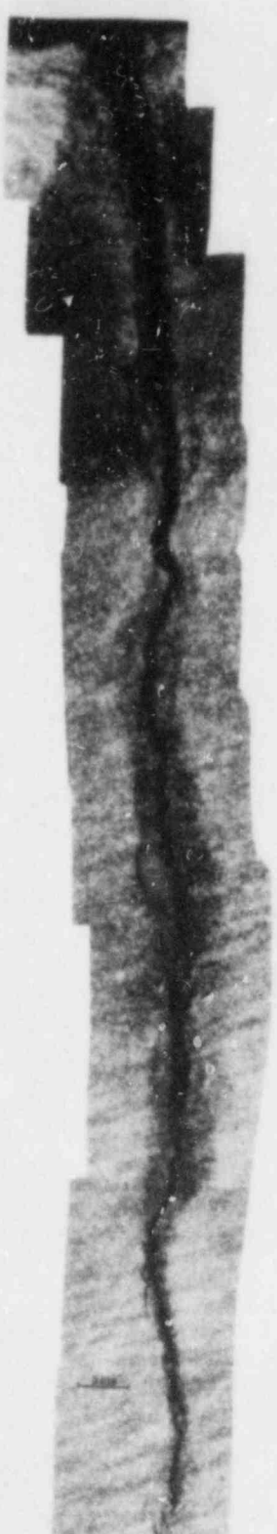

62.5X

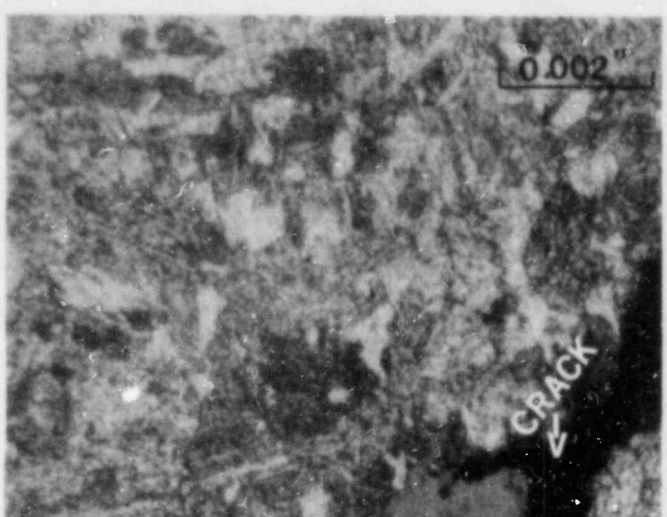

400X

21a: Base metal.

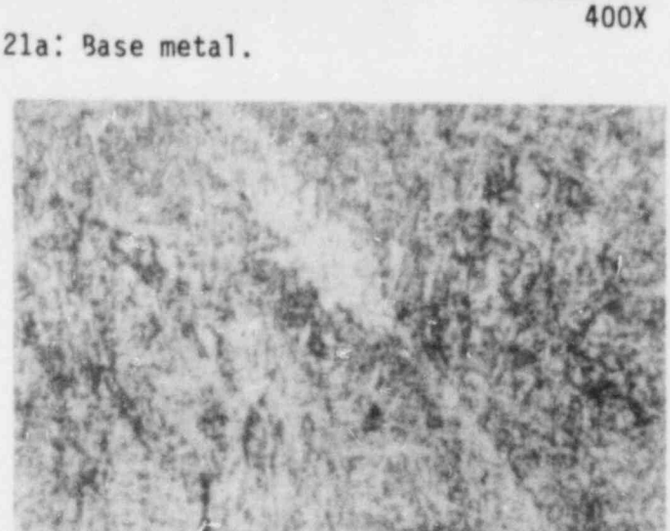

400X

21b. Weld metal

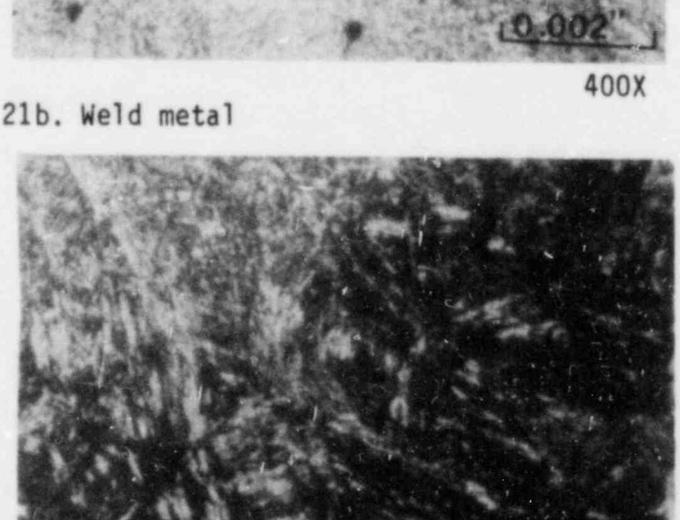

400X

21c. Heat affected zone.

Figure 21. Photomicrographs of the MT 37/38 crack. Higher mag. photos of the areas of interest are also shown.

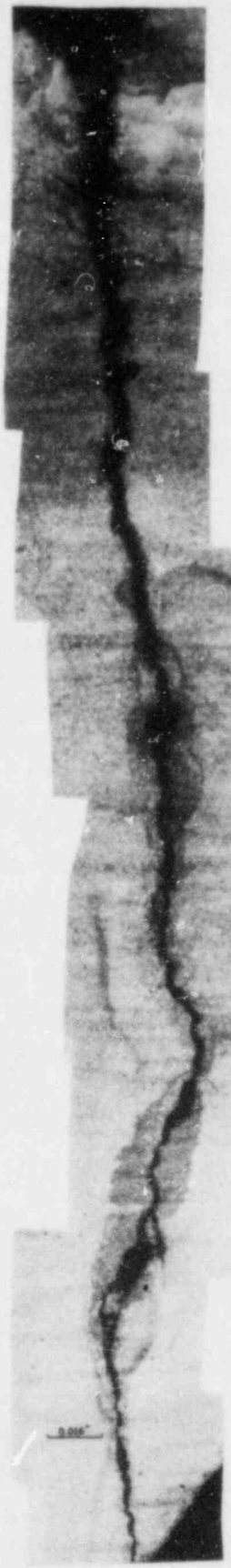

62.5X

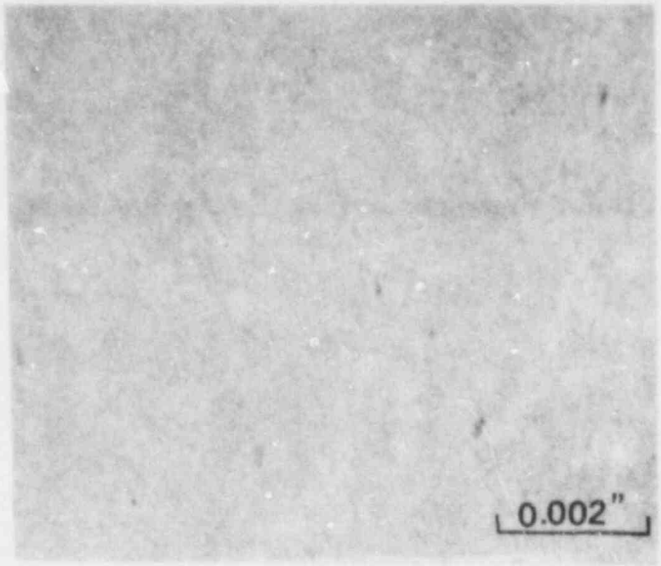

400X

22a. Base metal.

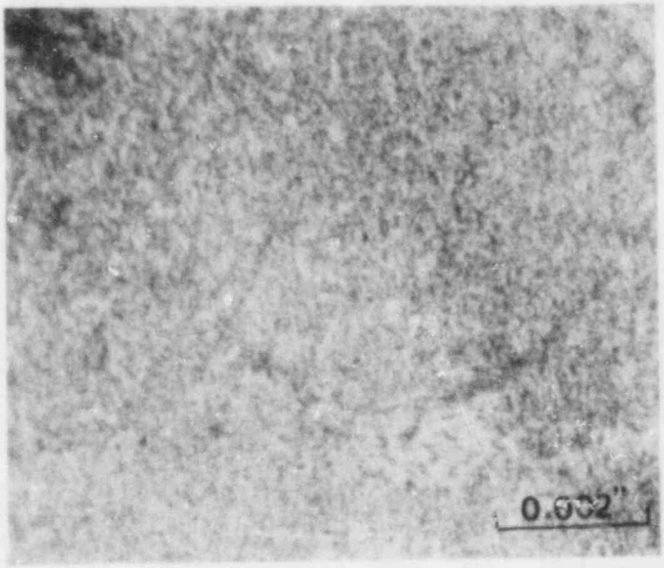

400X

22b. Weld metal

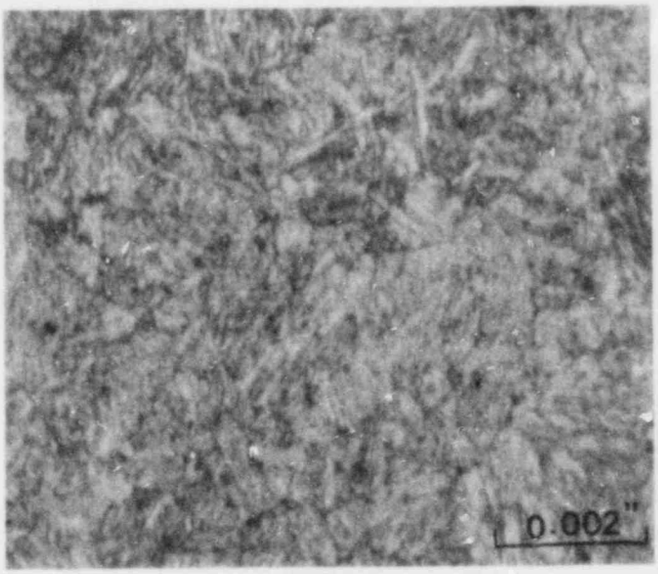

400X

22c. Heat affected zone.

Figure 22. Photomicrographs of the MT 44 crack. Higher mag.photos of the areas of interest are also shown.

62.5X

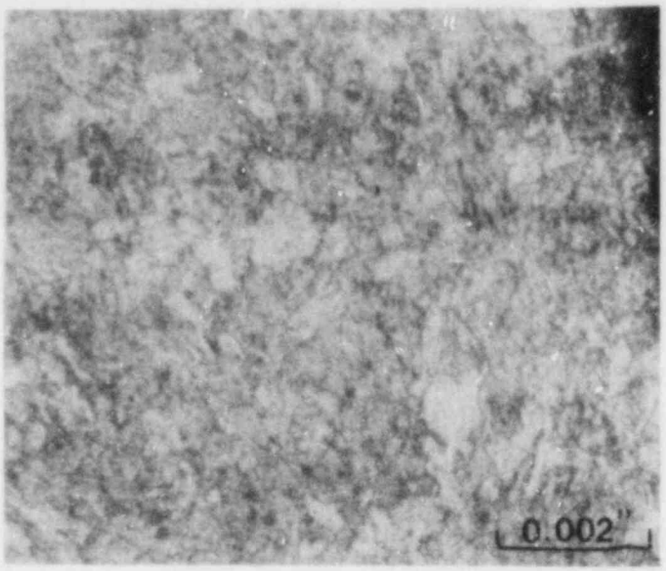

400X

23a. Base metal.

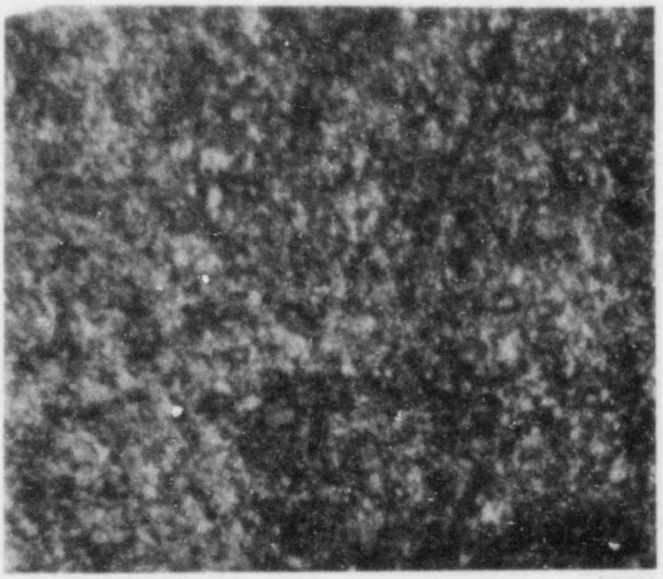

400X

23b. Weld metal.

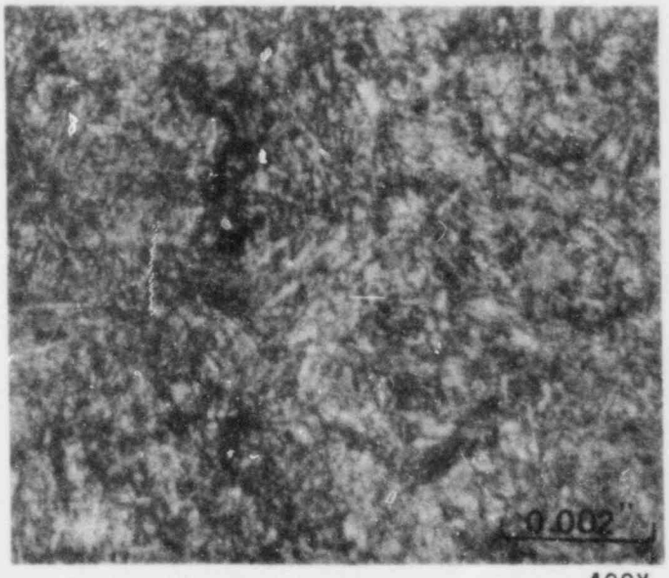

400X

23c. Heat affected zone.

Figure 23. Photomicrographs of the MT 46 crack. Higher mag.photos of the areas of interest are also shown.

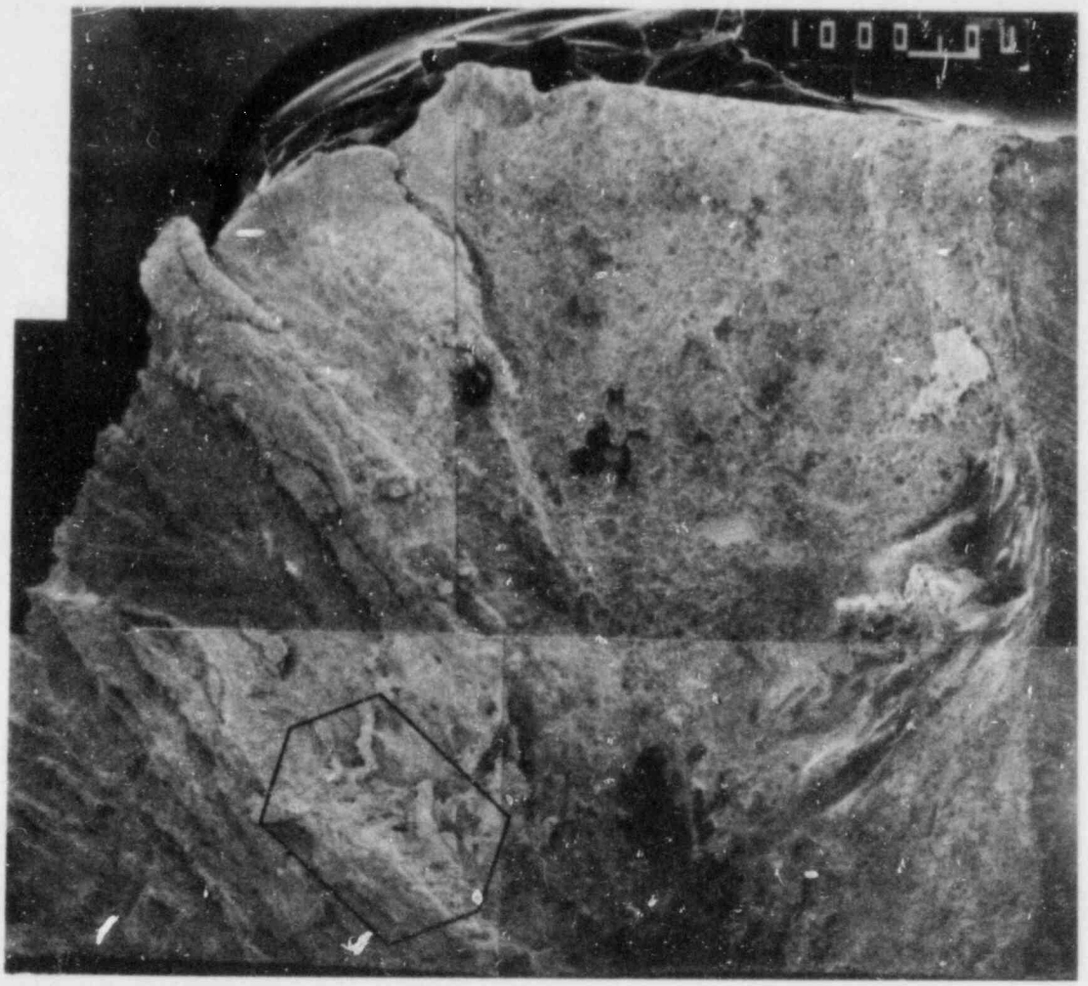

10X

Figure 24. SEM fractograph of the fracture face of an area of the "through wall leaker". The boxed area is one of the deposited copper locations.

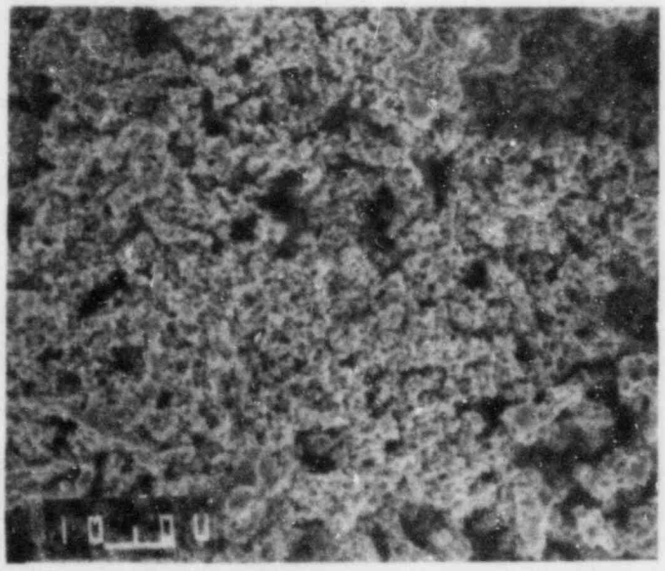

1000X

Figure 25a. Higher magnification photo of the copper deposit.

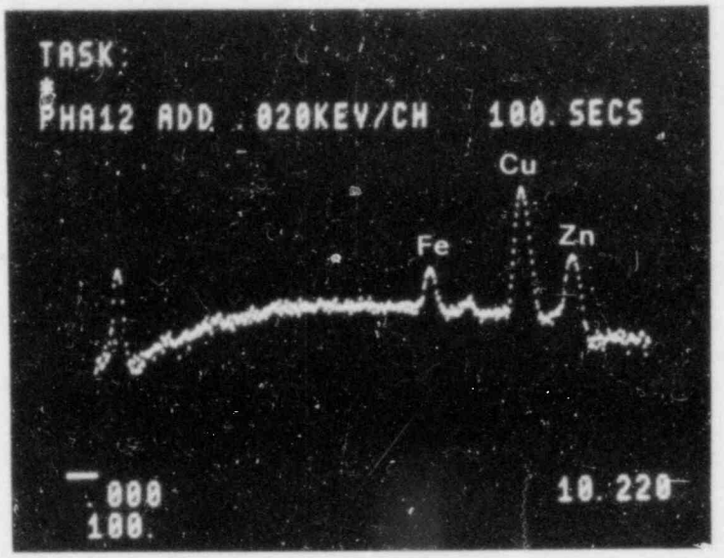

Figure 25b. EDS scan of the deposit in 25a showing a definite copper and zinc peak in addition to iron.

Figure 26. Low magnification SEM fractograph of one of the fracture faces associated with the 6"plug sample.Area "A" is an area of possible fatigue interaction while location"B" is an area of crack redirection.

Figure 27a. Fractograph of the area"A" in Fig.26 showing possible fatigue striations.Note the intimation of progressive fatigue characteristics.

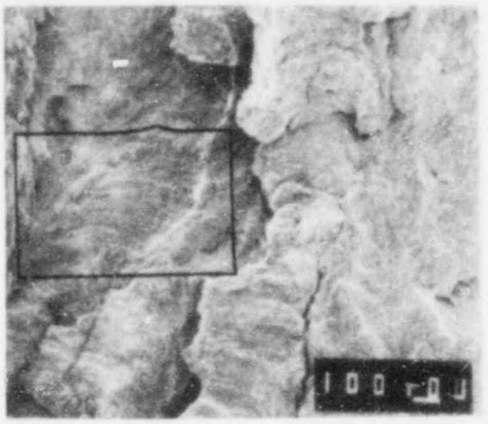

27b. Low magnification photo of area in 27a.

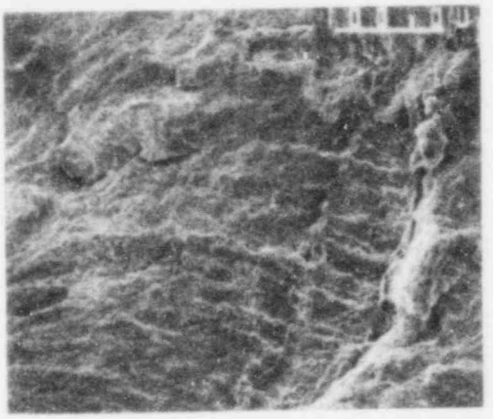

27c. Higher magnification photo of same area showing definite regular spacing of striations.

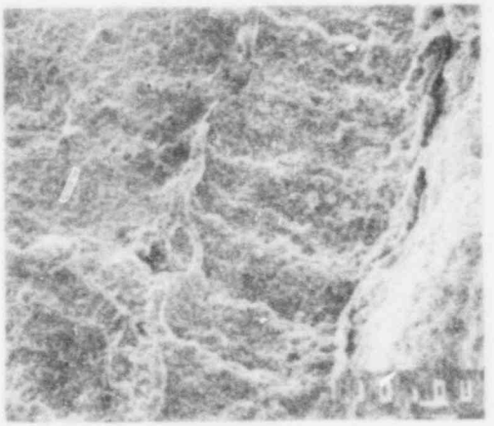

27d. High magnification photo of the same area.

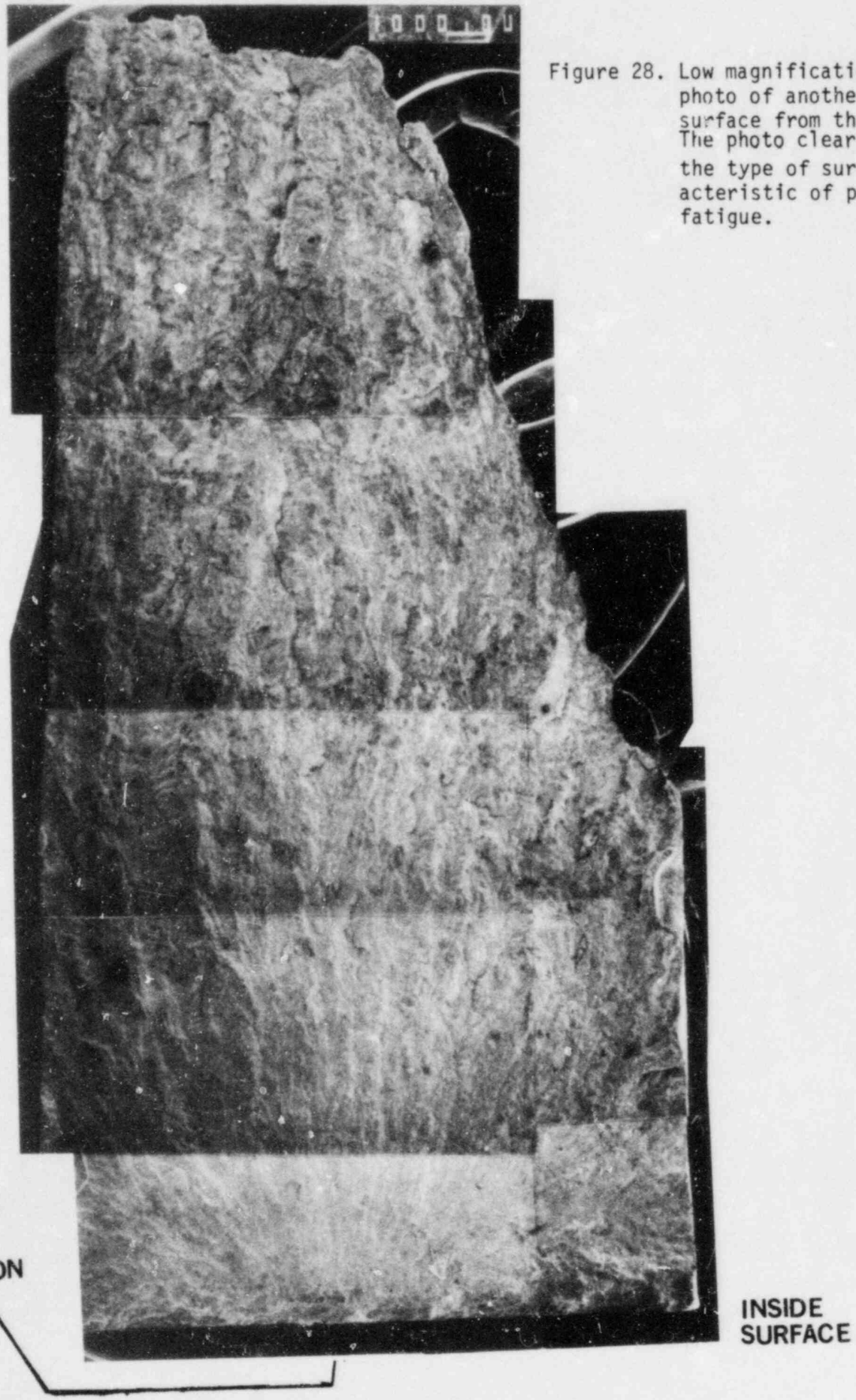

Figure 28. Low magnification SEM photo of another fracture surface from the 6"plug. The photo clearly depicts the type of surface characteristic of progressive fatigue.

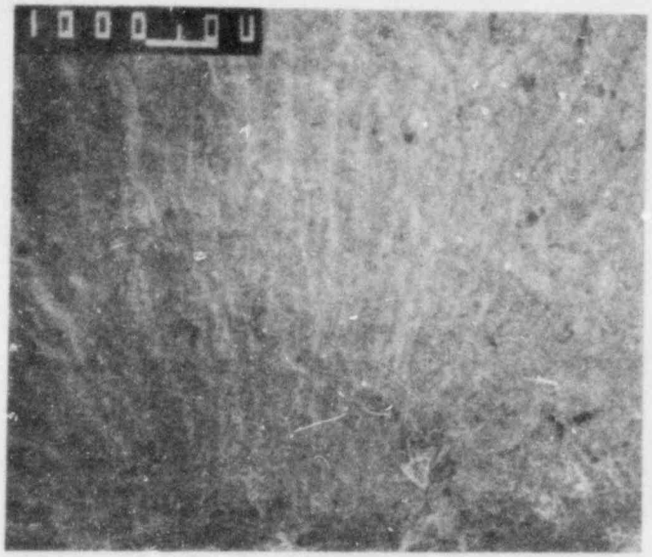

10X

Figure 29. An SEM fractograph showing definite indications of "beach marks" on the fracture surface.

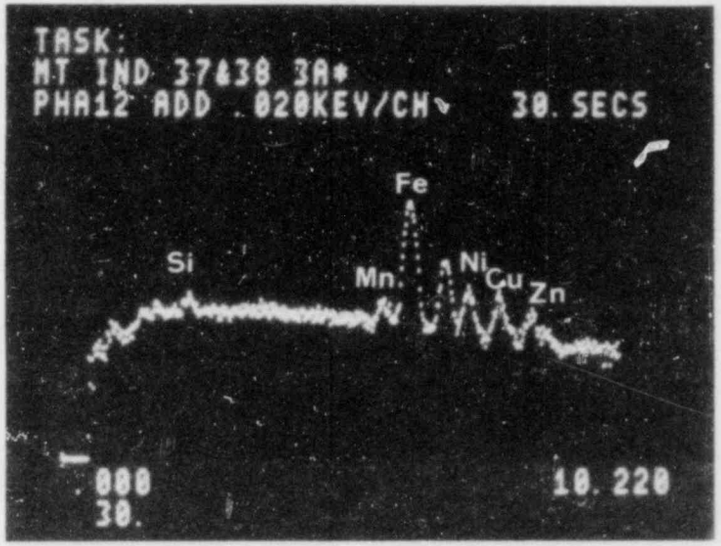

Figure 30. EDS scan of the fracture surface of specimen MT 37/38, depicting the typical elements found on the surface of the fracture.

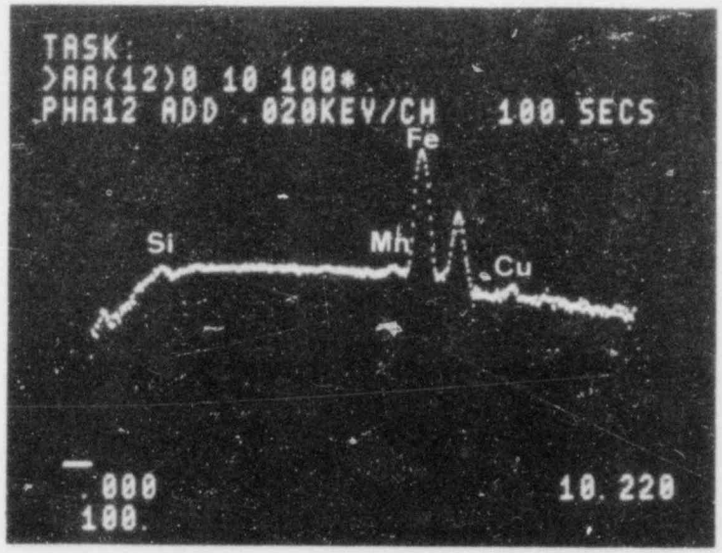

Figure 31. EDS scan of the fracture surface of specimen MT 44 for typical elements present.

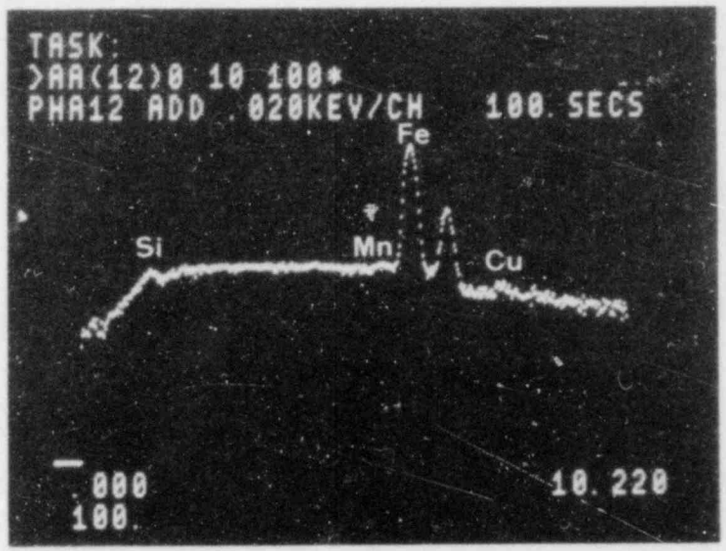

Figure 32. EDS scan for chemical constituents on specimen MT 46 fracture face.

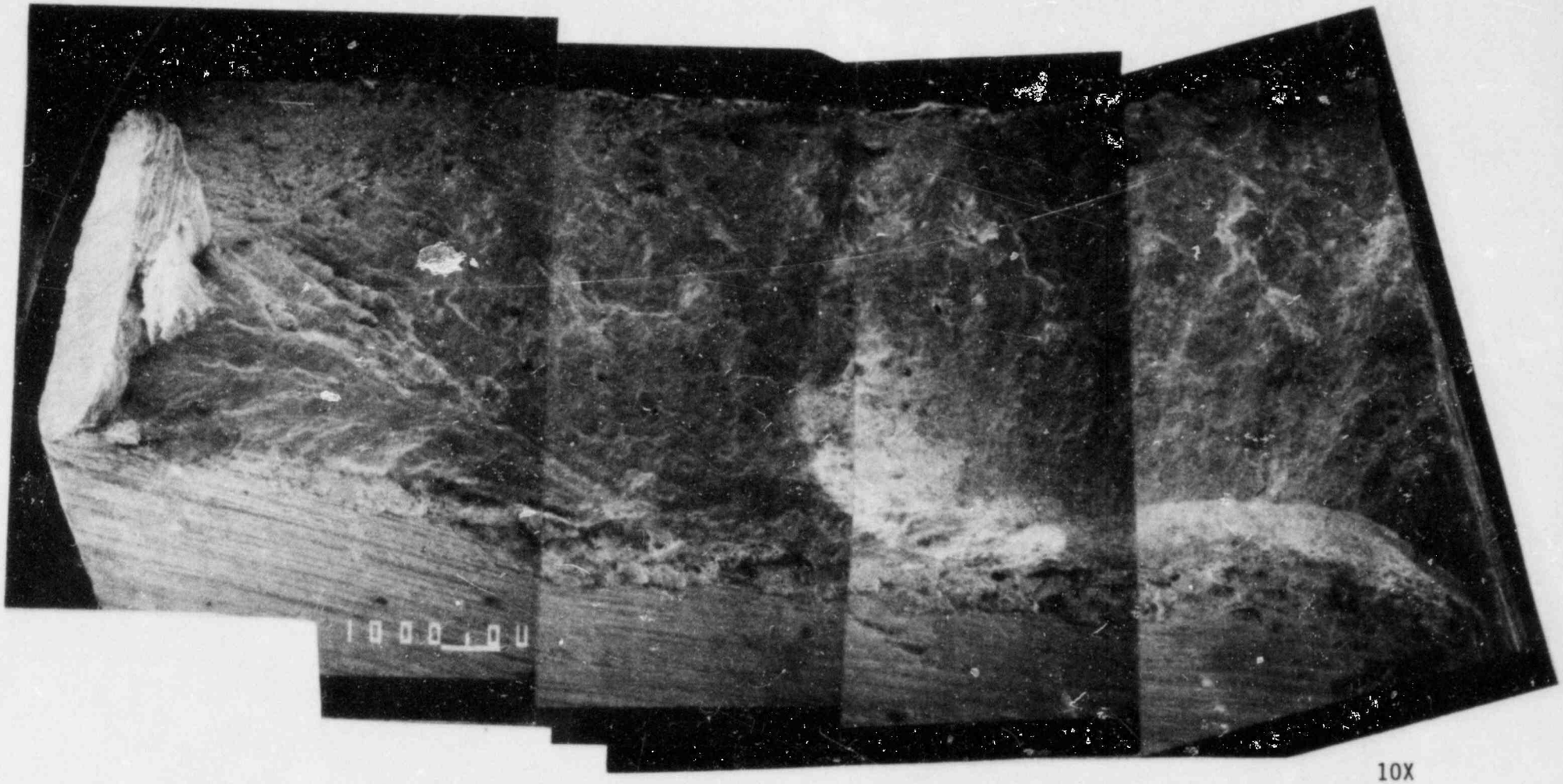

Figure 33. Low magnification fractograph of the fracture face on specimen MT 44, after electrolytic cleaning. The initiation site of the fracture originated on the inside surface of the steam generator, where a considerable amount of pitting is visible.

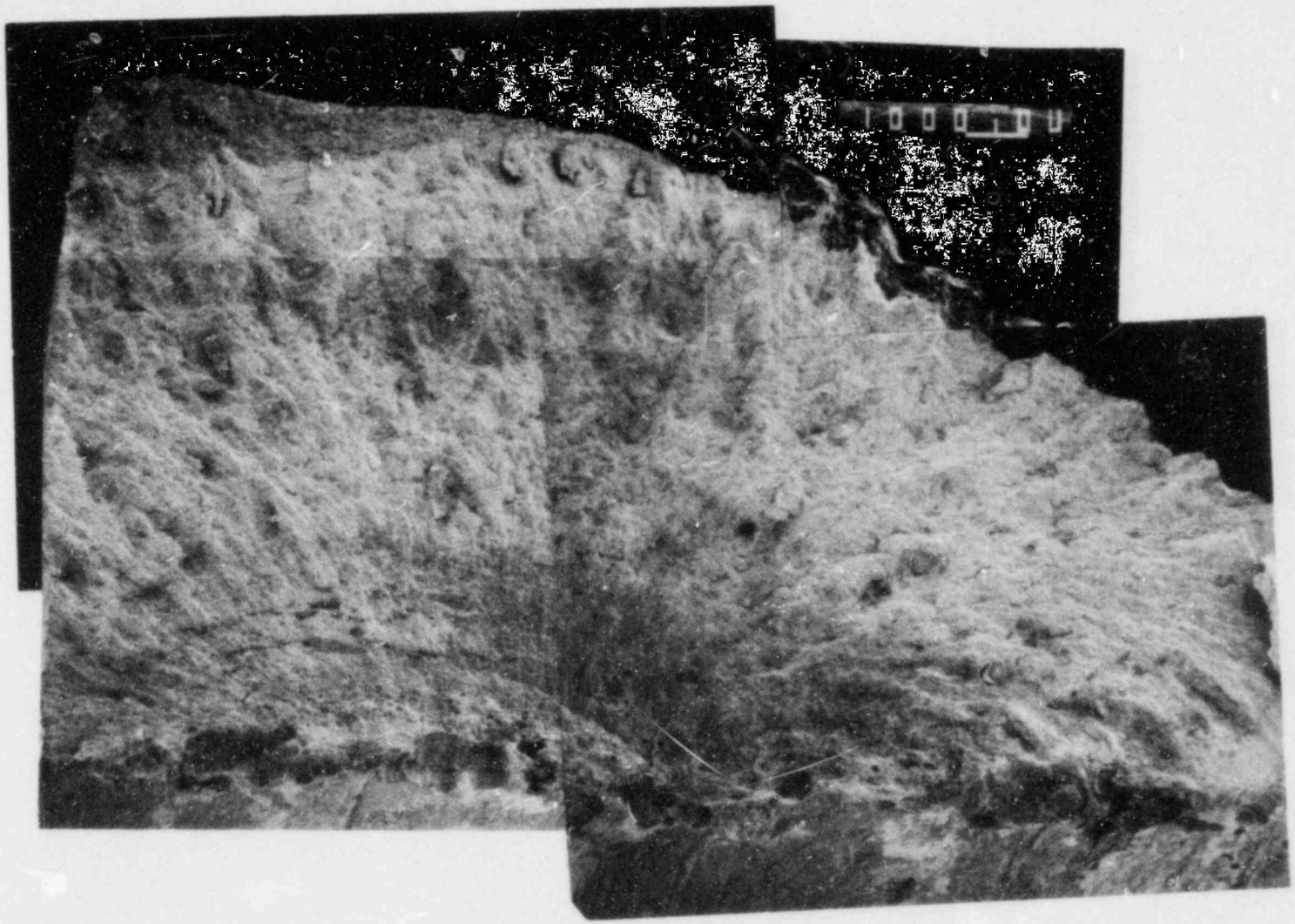

10X

Figure 34. SEM fractograph depicting the fracture face of specimen MT 46. The photgraph clearly shows the crack initiated at pits on the inside surface of the steam generator and has the general characteristics of a progressive or fatigue-like fracture.

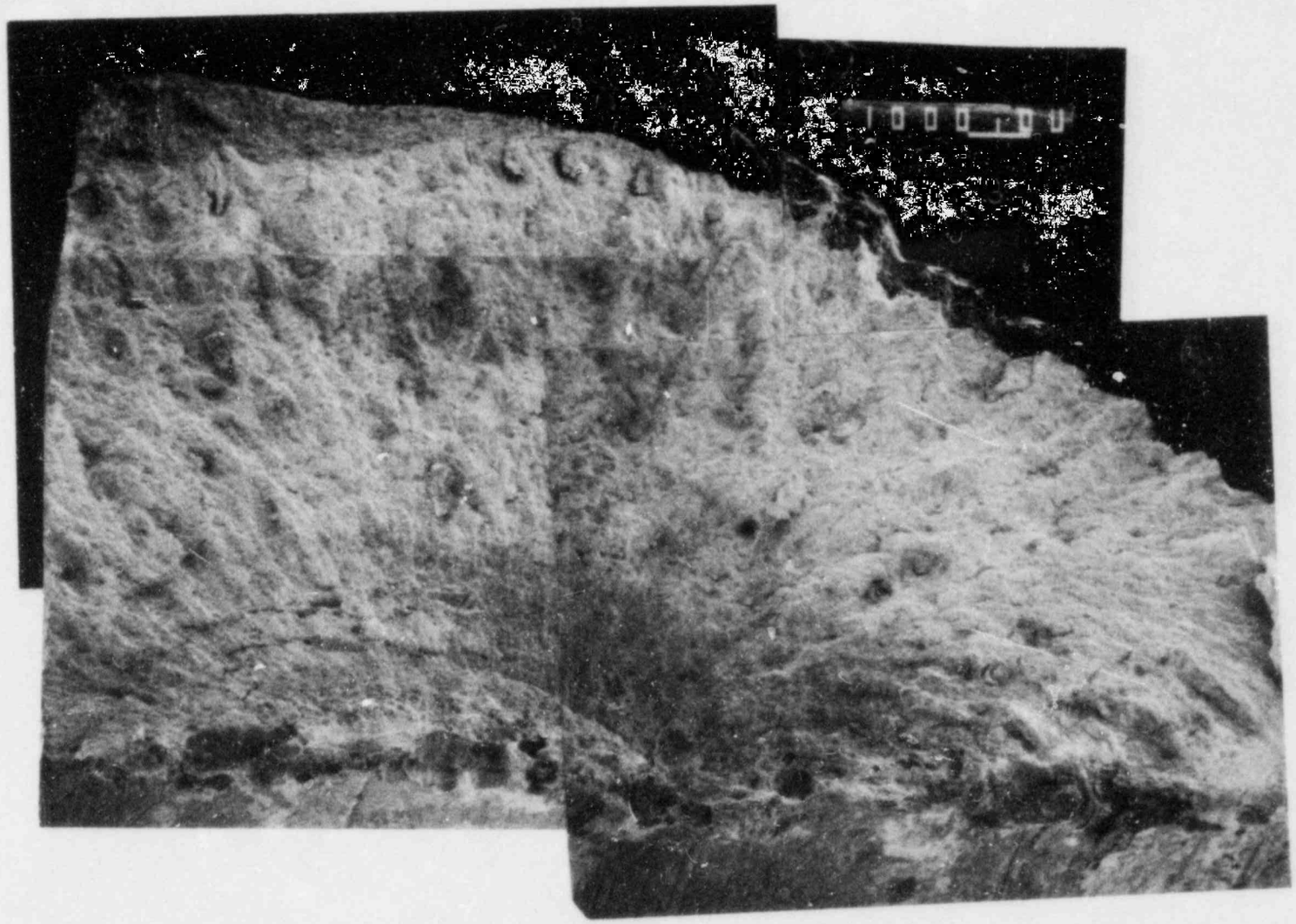

Figure 34. SEM fractograph depicting the fracture face of specimen MT 46. The photgraph clearly shows the crack initiated at pits on the inside surface of the steam generator and has the general characteristics of a progressive or fatigue-like fracture.

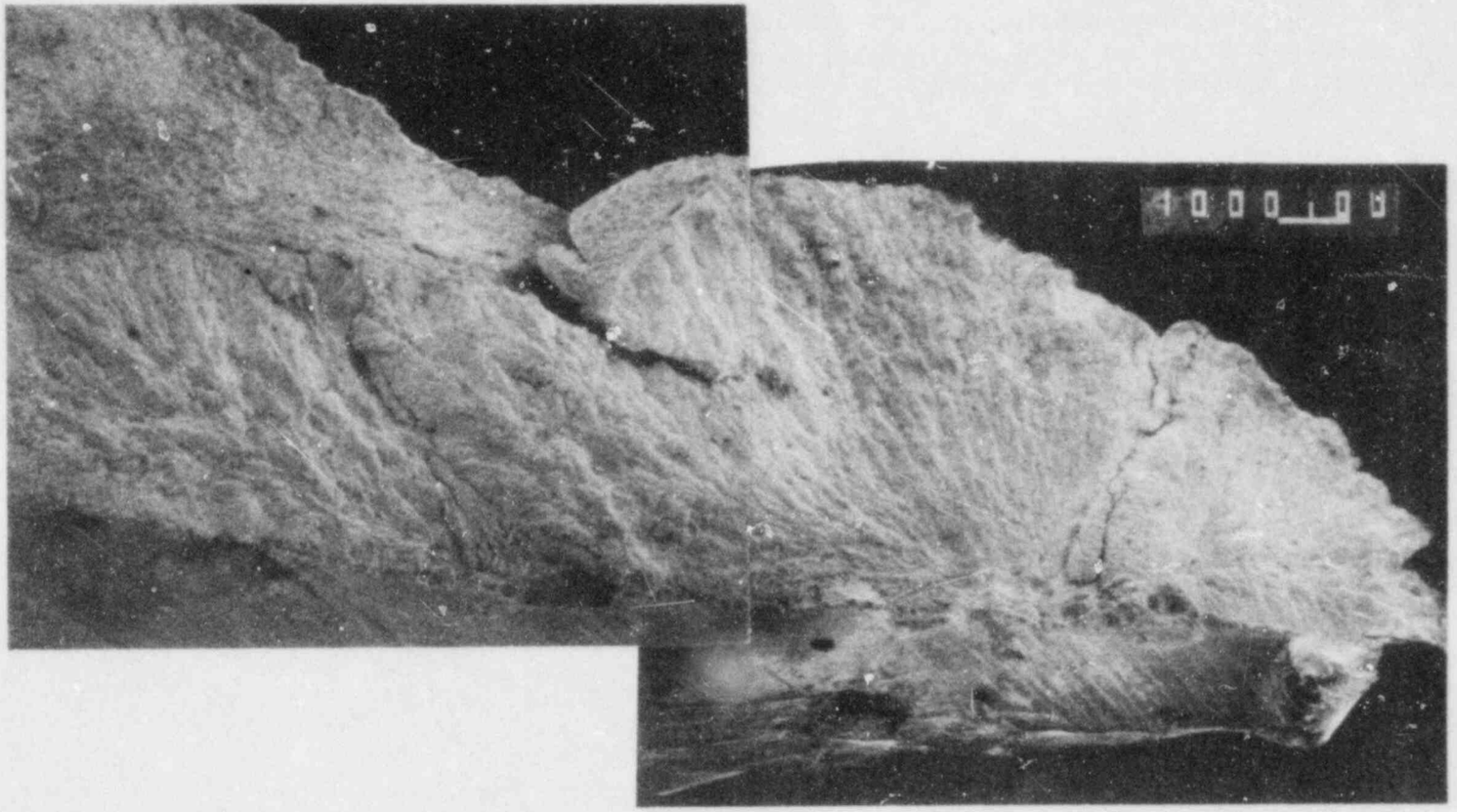

10X

Figure 35. Fractograph of the fracture face on specimen MT 37/38. The fractograph clearly has the "wood-like" structure characteristic of progressive or fatigue cracking. The photo also shows the initiation site to be on the steam generator's inside surface and apparently emanating from surface pitting.

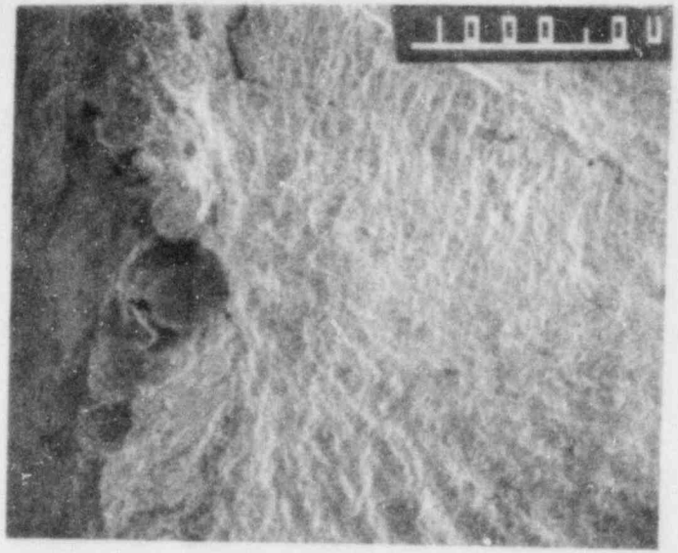

30X

Figure 36. SEM photo of the initiation site for specimen MT 37/38 showing the fatigue-like nature of the crack.

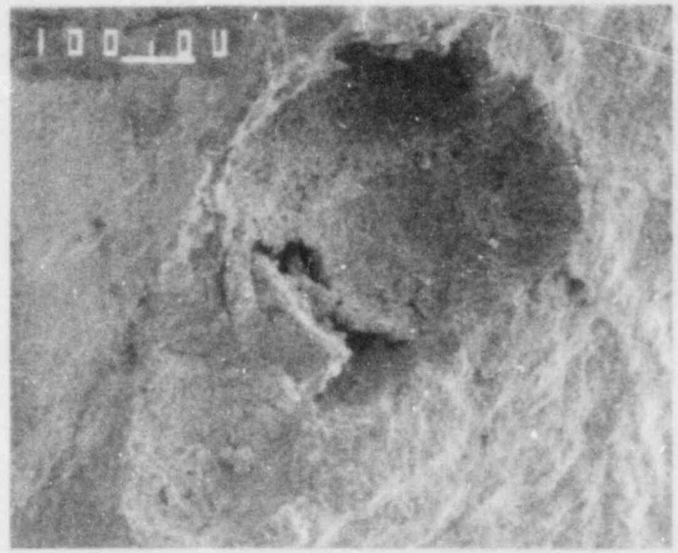

1000X

Figure 37a. Higher magnification photo of the pit in Fig. 36.

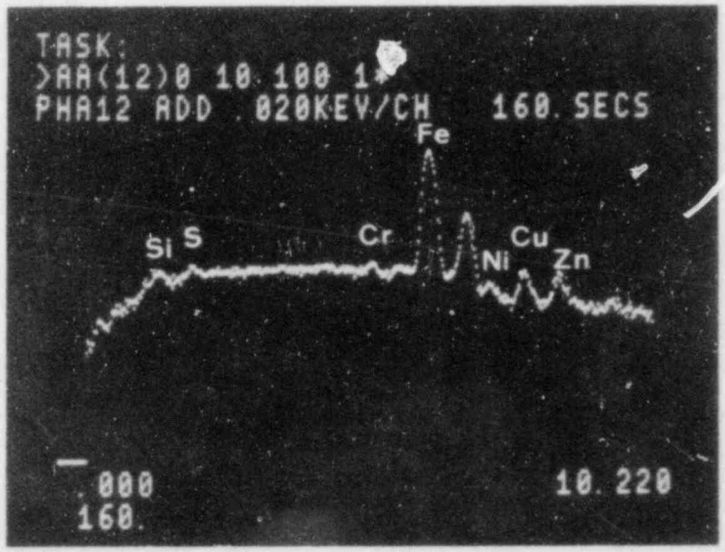

37b. EDS scan of the fracture surface of MT 37/38 showing constituents found near the initiation point.

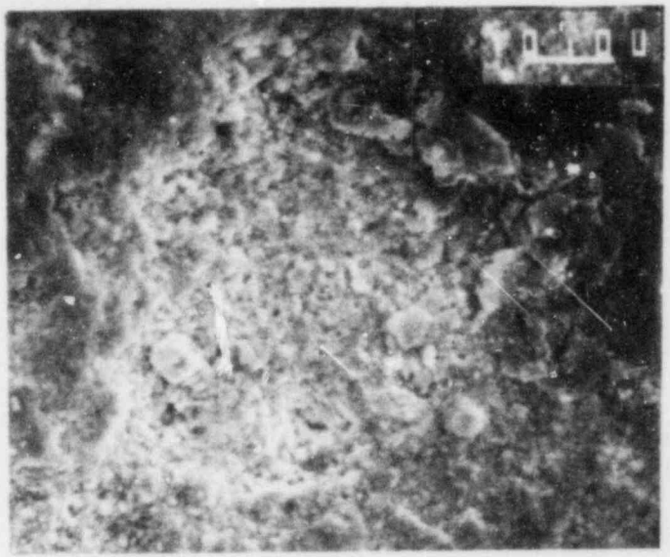

1200X

Figure 38a. SEM photo of the start of a pit found on the fracture face of specimen MT 44.

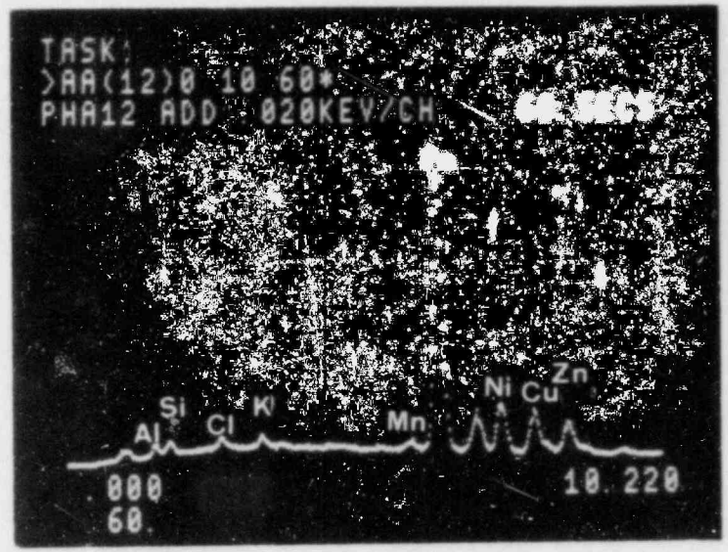

38b. EDS scan of the elements found in the vicinity of Fig. 38a.

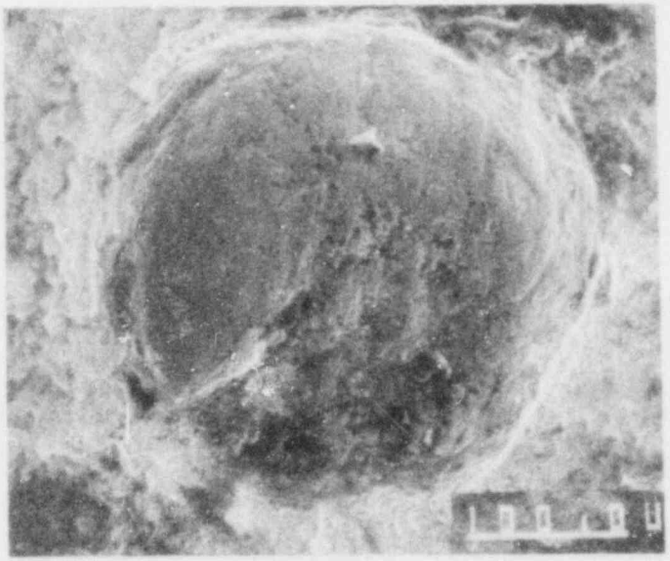

220X

Figure 39a. SEM photo of a pit found on the specimen MT 46.

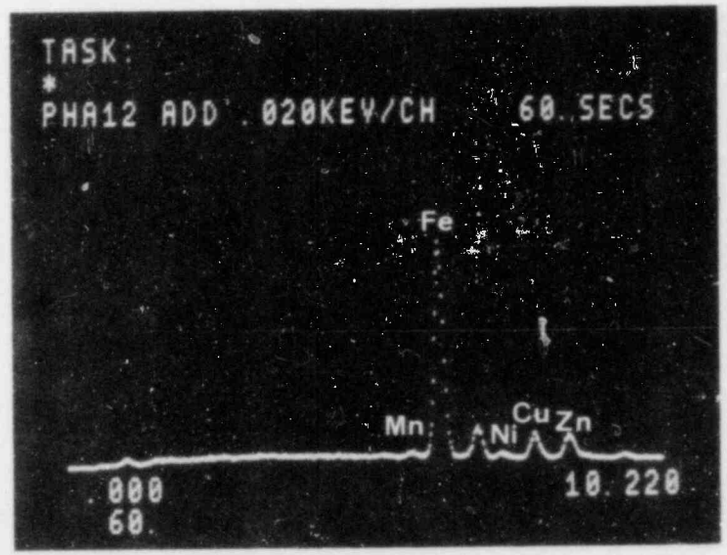

39b. EDS scan of the surface for constituents.

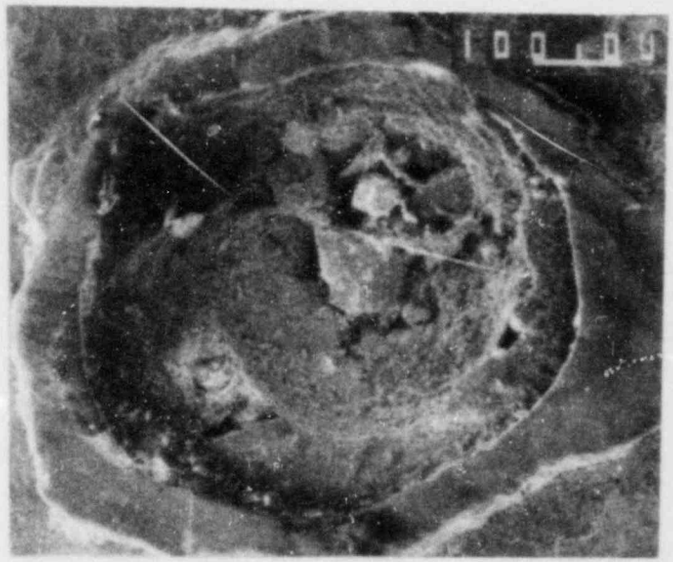

120X

Figure 40a. SEM photo of a pit found on the inside surface of the MT 37/38 specimen.

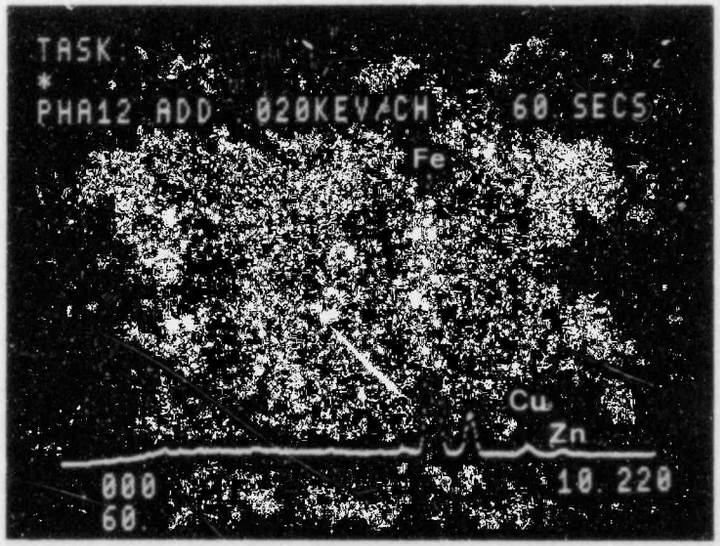

40b. EDS scan of the rim of the pit.

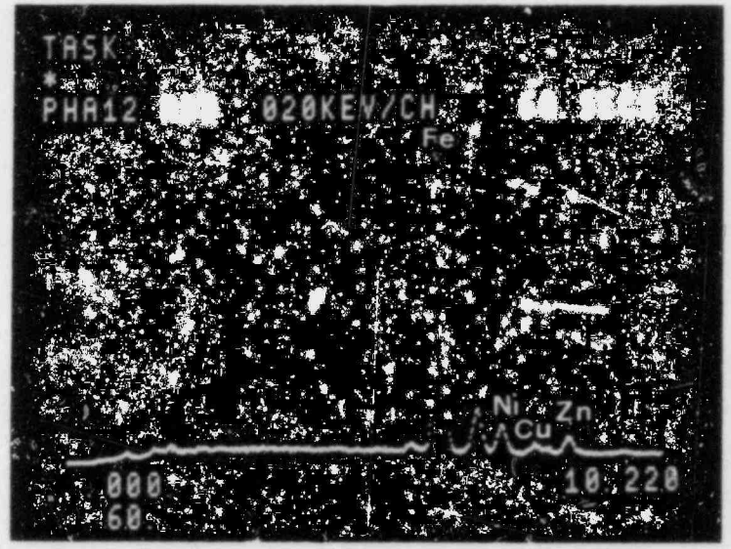

40c. EDS scan of the interior of the pit. Note the presence of Ni on this scan.

NRC FORM 335 (7 77) U.S. NUCLEAR REGULATORY COMMISSION

BIBLIOGRAPHIC DATA SHEET

1. REPORT NUMBER (Assigned by DDC)
NUREG/CR- 3281
BNL/NUREG- 51670

4. TITLE AND SUBTITLE (Add Volume No., if appropriate)
INVESTIGATION OF THE SHELL CRACKING ON THE STEAM GENERATORS OF INDIAN POINT #3

2. (Leave blank)

3. RECIPIENT'S ACCESSION NO.

7. AUTHOR(S)
Carl J. Czajkowski

5. DATE REPORT COMPLETED
MONTH: April YEAR: 1983

9. PERFORMING ORGANIZATION NAME AND MAILING ADDRESS (Include Zip Code)
Brookhaven National Laboratory
Department of Nuclear Energy
Upton, New York 11973

DATE REPORT ISSUED
MONTH: June YEAR: 1983

6. (Leave blank)

8. (Leave blank)

12. SPONSORING ORGANIZATION NAME AND MAILING ADDRESS (Include Zip Code)
Division of Engineering
Office of Nuclear Reactor Regulation
U.S. Nuclear Regulatory Commission
Washington, D.C. 20555

10. PROJECT/TASK/WORK UNIT NO

11. CONTRACT NO.
FIN A-3400

13. TYPE OF REPORT
Technical

PERIOD COVERED (Inclusive dates)

15. SUPPLEMENTARY NOTES

14. (Leave blank)

16. ABSTRACT (200 words or less)

A metallurgical investigation was performed on specimens from the shell of steam generacors #31 and 32 of the Indian Point 3 Power Plant. The examination consisted of optical microscopy, SEM/EDS, hardness measurements, and two different heat treatments. The shell material exhibited high values in hardness prior to the heat treatments, which was indicative that relatively high residual stresses may have been present in the areas of the welds. All observed cracks were transgranular in appearance and were associated with pits on the vessel's inside surfaces. The report concludes that the cracking was caused by a low cycle corrosion fatigue phenomenon with cracks initiating at areas of localized corrosion and propagating by fatigue.

17. KEY WORDS AND DOCUMENT ANALYSIS

17a. DESCRIPTORS

corrosion fatigue
shell cracking
transgranular cracking
pits

17b. IDENTIFIERS/OPEN-ENDED TERMS

18. AVAILABILITY STATEMENT
Unlimited

19. SECURITY CLASS (This report)
Unclassified

21. NO. OF PAGES

20. SECURITY CLASS (This page)
Unclassified

22. PRICE
$

NRC FORM 335 (7 77)

NUREG/CR-3281 INVESTIGATION OF SHELL CRACKING ON THE STEAM GENERATORS AT INDIAN POINT UNIT NO. 3 JUNE 1983